

The Pennsylvania State University

The Graduate School

College of Engineering

**MATHEMATICAL MODELS OF BRAIN AND CEREBROSPINAL FLUID DYNAMICS:
APPLICATION TO HYDROCEPHALUS**

A Thesis in

Engineering Science and Mechanics

by

Justin Kauffman

© 2013 Justin Kauffman

Submitted in Partial Fulfillment
of the Requirements
for the Degree of

Master of Science

May 2013

The thesis of Justin Kauffman was reviewed and approved* by the following:

Corina Drapaca
Associate Professor of Engineering Science and Mechanics
Thesis Advisor

Francesco Costanzo
Professor of Engineering Science and Mechanics

Albert Segall
Professor of Engineering Science and Mechanics

Judith Todd
P.B. Breneman Department Head Chair
Head of the Department of Engineering Science and Mechanics

*Signatures are on file in the Graduate School

ABSTRACT

Hydrocephalus is a serious neurological disorder characterized by abnormalities in the circulation of cerebrospinal fluid (CSF). Hydrocephalus results from an excessive accumulation of CSF in the ventricles of the brain, brain compression, and sometimes an increase in the intracranial pressure. It is believed that hydrocephalus is either caused by an increase in CSF production, or by an obstruction of the circulation of CSF or of the venous outflow system. The treatment is therefore based on CSF flow diversion. Given that the response of the patients who have been treated continues to be poor there is an urgent need to design better therapy protocols for hydrocephalus. Mathematical models of CSF dynamics and CSF-brain interactions could play important roles in the design of improved, patient-specific treatments. One of the first predictive mathematical models of CSF pressure-volume interactions was proposed by Marmarou in the 1970's and provides a theoretical basis for studying hydrocephalus. However, this model fails to fully capture the complexity of the CSF dynamics. In this thesis we will propose a generalization to Marmarou's model using fractional calculus. We use a modified Adomian decomposition method to solve analytically the proposed fractional order nonlinear differential equation. Our results show temporal multi-scaling behavior of CSF dynamics. In addition, we also propose a novel coupled-field model using Hamilton's principle to capture some of the dynamics taking place at the macroscopic and microscopic scales during the onset and evolution of hydrocephalus. Our coupled-field model introduces healing (growth) and inflammation (aging) states of the brain which show distinct temporal variations when we use experimentally measured volumetric data for healthy and hydrocephalic mice.

TABLE OF CONTENTS

List of Figures	v
List of Tables	vi
Acknowledgements.....	vii
Chapter 1 Introduction	1
Chapter 2 Literature Review	4
2.1 Hakim Model.....	4
2.2 Marmarou Model.....	7
2.3 Fractional Calculus.....	10
2.4 Adomian Method.....	12
Chapter 3 Fractional Marmarou Model	15
3.1 Classic Marmarou Model	15
3.2 Fractional Linear Marmarou Model	18
3.3 Fractional Nonlinear Marmarou Model	21
3.4 Results	26
3.5 Concluding Remarks	29
Chapter 4 Stress Strain Analysis in a Cylindrical Geometry with Applications to Brain- CSF Interactions.....	35
4.1 Theory	35
4.2 Results	42
Chapter 5 Brain Biomechanics using Hamilton’s Principle	44
5.1 Theory	44
5.2 Application to Hydrocephalus.....	48
Chapter 6 Conclusions and Future Work.....	53
Appendix A MATLAB Code.....	55
Bibliography	67

LIST OF FIGURES

Figure 1: Pathway of CSF flow in the brain, adapted from [9].....	5
Figure 2: The Rectilinear Model.....	5
Figure 3: The Spherical Model	6
Figure 4: Analytic Solution of Equation (2.2.2) for the bolus injection case.	9
Figure 5: Analytic solution of Equation (2.2.2) for the continuous infusion case.	9
Figure 6: Analytic Solution of Equation (2.2.2) for the case of volume removal.....	10
Figure 7: Shape of CSF pressure for the case of constant infusion for the following values of α : 0.25(-), 0.5 (+), 0.75 (*), 0.95 (--). The solid line corresponds to the solution given by Equation (3.1.5).....	27
Figure 8: In the case of bolus injection, the CSF pressure found in [1] is shown as a solid line, while the dashed blue line shows the CSF pressure calculated using a sequence of continuous functions to approximate the Dirac distribution.....	27
Figure 9: The shapes of the CSF pressure for the case of bolus injection for the following values of α : a) 0.05 (-), 0.15(+), 0.25 (*), 0.35 (--). The solid line shows our approximate solutions to Marmarou's model in this case. The largest radius of convergence corresponds to $\alpha = 0.35$ and is given by $\rho_2 = 0.4754$, and b) 0.25 (-), 0.5 (+), 0.75 (*), 0.95 (--). The solid line shows our approximate solutions to Marmarou's model in this case. The largest radius of convergence corresponds to $\alpha = 0.95$ and is given by $\rho_2 = 1.0983$	29
Figure 10: Axi-symmetrical stress distribution in a hollow cylinder under uniform pressure on the inner and outer surfaces.	38
Figure 11: Fractional linear case for bolus injection for α values of: 0.25 (-), 0.5 (+), 0.75 (*), 0.95 (--), 1 (solid). The solid line represents the classical solution.....	42
Figure 12: Fractional nonlinear case for bolus injection for α values of: 0.25 (-), 0.5 (+), 0.75 (*), 0.95 (--), 1 (solid). The solid line represents the classical solution.....	43
Figure 13: Jacobian for (a) normal (red) and (b) hydrocephalic (blue) mice and their corresponding polynomial fits.....	50
Figure 14: Healing (red) and inflammation (blue) state functions versus time for the following initial conditions: a) – b) $\psi_h, \psi_i, v_h, v_i = 1, 0, 0, \text{eps}$; c) – d) $\psi_h, \psi_i, v_h, v_i = 1, 0, 0.1, \text{eps}$; e) – f) $\psi_h, \psi_i, v_h, v_i = 0, 1, -1, 1$. The first column represents the normal mice data, while the second column shows the hydrocephalic mice data. In Matlab $\text{eps} = 2.2204e - 016$	51

LIST OF TABLES

Table 1: Analytic Solutions to equation (2.2.1) for the three different cases presented in [1]. Note that is P_t the threshold pressure.	8
Table 2: Calculated Jacobians from brain volumetric data for normal and hydrocephalic mice.	49

ACKNOWLEDGEMENTS

I would like to thank Dr. Corina Drapaca for all the support and help she has given me the past two years. None of this would have been possible without that support. I would also like to thank my committee members, Dr. Francesco Costanzo and Dr. Albert Segall, for their comments and suggestions that helped improve my thesis.

I would also like to thank my parents, Chuck and Diane Kauffman, and my girlfriend, Danielle Smith, who have always helped motivate me and never let me get discouraged.

I would finally like thank the Engineering Science and Mechanics department for allowing me to continue my education and allowing me to meet my goals.

Chapter 1

Introduction

Hydrocephalus is a serious neurological disease that develops from abnormalities in the circulation of cerebrospinal fluid (CSF). It results in ventricular dilation, compression of the brain and a possible increase in intracranial pressure (ICP). Although hydrocephalus is one of the most common neurological disorders treated by neurosurgeons, the cause of hydrocephalus is still unknown because it can develop in conjunction with other neurological disorders, or even infections resulting in inflammation of the brain.

The treatment of hydrocephalus is primarily based on diverting the CSF flow such that the symptoms of the disease are reduced. This can be accomplished surgically by either implanting a shunt into the ventricles or a procedure called endoscopic third ventriculostomy (ETV). An implanted shunt redirects some of the excess CSF through a tube to the patient's stomach causing a decrease in the volume of the ventricles. However, shunt implantation has a high risk of infection. On the other hand, ETV drains the ventricles through a hole made in the third ventricle. In time this hole closes and a new surgery is often required. Clinical studies have shown that neither of these treatments is effectively treating hydrocephalus. Shunts tend to be a lifelong implant and tend to fail frequently among patients, while ETV is usually done only in patients with a minimal risk in ventricular dilation in the future. Knowledge of the mechanics of brain-ventricular CSF interface and the CSF circulation can help neurosurgeons determine which treatment would result in a better outcome for a specific patient.

In order to improve the outcome of treatment and design new and better therapies for hydrocephalus, we could benefit tremendously from accurate mathematical models describing the

CSF dynamics and CSF-brain interactions. Such models could help us understand the fundamental science behind hydrocephalus. *Marmarou et. al.*, [1] and *Hakim et. al.*, [2] developed the first models describing hydrocephalus. Marmarou modeled the CSF dynamics and used experiments in cats to validate his model; whereas Hakim looked at the brain as a viscoelastic material and proposed an engineering approach to explain the onset and evolution of hydrocephalus using a series of controlled experiments. In this thesis we will develop a multi-scale pressure-volume model describing the CSF dynamics. We will generalize Marmarou's model by using fractional calculus, and by doing this, we understand that we are changing the physical meaning behind the original model. By using a fractional order temporal derivative we introduce an inhomogeneous clock that connects continuously the global (macroscopic) time scale to the local (microscopic) time scale. We solve our fractional differential equation analytically using a modified Adomian decomposition method described in *Duan et. al.*, [3]. We compare our results to Marmarou's classical solution and then use numerical simulations to show the changes in displacement of the brain-ventricular CSF interface.

This thesis is structured as follows. Chapter 2 will be a brief review of Marmarou's and Hakim's models followed by an introduction of fractional calculus and its application to neuronal activity, and a description of the Adomian decomposition method used to analytically solve our differential equations. In chapter 3 we will describe the classical Marmarou model, introduce our fractional Marmarou model and compare the two models. We assume a cylindrical geometry of the brain parenchyma and show the displacement fields of the brain-ventricular CSF interface corresponding to the classic and fractional Marmarou models in Chapter 4. For the sake of completeness, a presentation of the classic stress-strain analysis in a cylindrical domain is also given in Chapter 4. Finally, in Chapter 5 we propose a totally different approach to studying hydrocephalus. We introduce two states of the brain, healing (growth) and inflammation (aging), and then invoke Hamilton's principle, and investigate the interplay between these two states using

experimentally found brain volumetric data for healthy and hydrocephalic mice. Our preliminary results show that inflammation overpowers healing in the case of untreated hydrocephalic mice, while in the case of healthy aging mice, inflammation grows slowly with age and the healing decreases as one would expect. The thesis ends with a chapter on conclusions and future work.

Our fractional Marmaou model will be published in [4, 5], while some of our work on the coupled-field model of brain biomechanics using Hamilton's principle will appear in [6].

Chapter 2

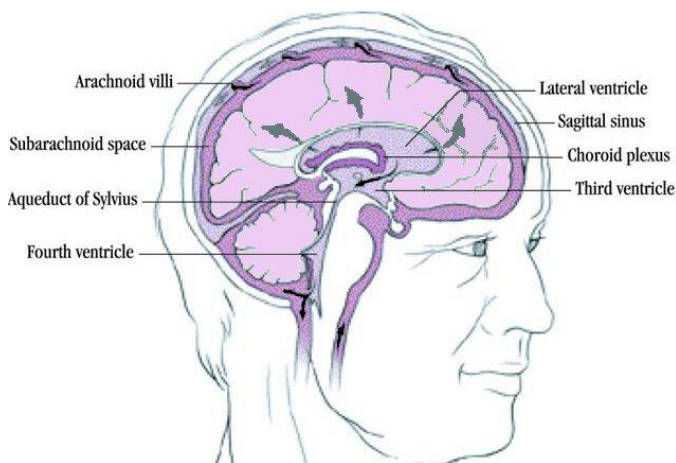
Literature Review

2.1 Hakim Model

Hakim et. al., [2] provided the first engineering approach to studying hydrocephalus¹. They had proposed a mathematical framework to study brain biomechanics along with simplistic engineering systems while using experiments from a purely mechanics point of view that explained the onset of hydrocephalus. The research that is presented in [2] is based on several years of medical evidence on CSF dynamics. CSF is produced by the choroid plexus which is located at the interface between the brain parenchyma and ventricles. Under normal conditions CSF is produced at a constant rate and decreases as we get older. Despite the fact that this knowledge is essential for hydrocephalus, we do not know the rate of CSF production and there are no realistic or robust methods or technologies to measure or estimate it [8].

Figure 1 shows the pathway of CSF flow through the brain. The flow of the CSF starts in the lateral and third ventricles and passes through the aqueduct of Sylvius to reach the fourth ventricle. Once the CSF gets through the fourth ventricle it circulates into the subarachnoid space [8]. A portion of the CSF flows down into the lumbar subarachnoid space; which, is believed to be the cause of pulsations [10]. The CSF is then absorbed by the arachnoid villi situated around the sagittal sinus [8]. It is not possible to undo absorption because the ICP is greater than the sagittal sinus pressure (P_{ss}). Another possibility for CSF drainage is that some of the CSF can “soak” through into the parenchyma [11].

¹ This section is adapted from [7]



The most common cause of hydrocephalus is an obstruction in the CSF flow. For example when there is a blockage between the third and fourth ventricles non-communicating hydrocephalus is developed and causes swelling to occur in the lateral

and third ventricles due to excess CSF accumulation [8]. This type of hydrocephalus is commonly treated with ETV, in which the third ventricle is punctured and the excess CSF is drained from the ventricles into a cistern part of the normal flow path. On the other hand communicating hydrocephalus is treated with shunts which drains the fluid through a tube into the patient's stomach.

Hakim et al., [2] describe the brain as being suspended in CSF and fixed into place from arachnoidal strands which connect the brain to the arachnoid membrane. The CSF is not compressing the brain but is instead providing hydrostatic forces that act as a support to allow it to oppose deformation. The brain parenchyma is seen to be like a submicroscopic sponge of almost incompressible viscoelastic material. This engineering point of view on the brain revolutionized this field of medicine since it contributed to the development of the shunts and hydrocephalus was finally treatable.

In their seminal work *Hakim et al.*, [2] proposed two simple mechanical models: a

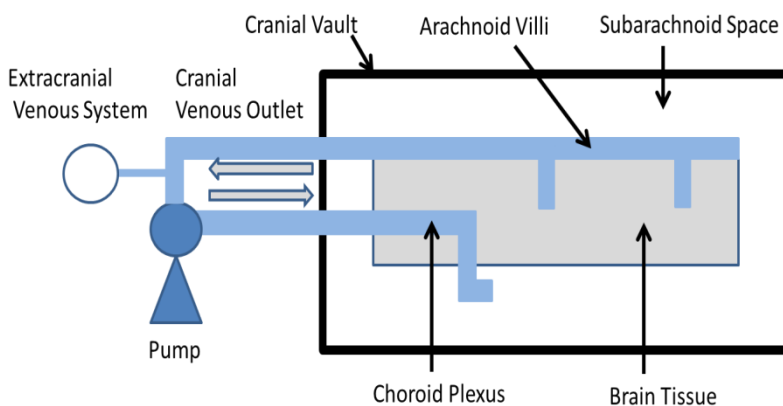


Figure 2: The Rectilinear Model

rectilinear model which was used to understand the CSF dynamics, and a spherical model which more accurately resembles the anatomical geometry of the brain. The rectilinear model (Figure 2) describes how an open venous system would interact with a closed CSF system [2]. This system looks at a small piece of the parenchymal sponge and establishes a relationship between the CSF and venous pressures. If both the CSF and venous pressures are increased simultaneously by the same amount then a uniform distribution of pressure is created inside the closed cranial cavity which will not allow either the sponge-like brain parenchyma to undergo any deformation or the CSF to be squeezed out of the tissue. However, when the CSF pressure is increased with respect to the venous pressure, the CSF will be pushed out of the brain tissue, causing a decrease in the volume of the brain parenchyma and thus allowing the increase of the ventricles. This last scenario is considered to model hydrocephalus.

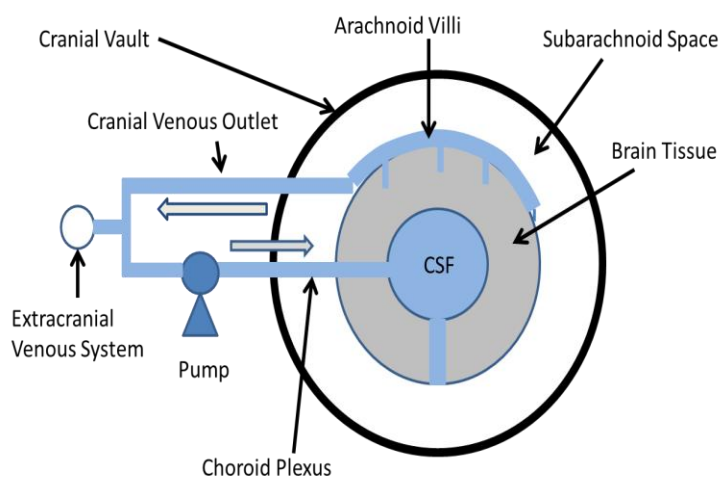


Figure 3: The Spherical Model

The spherical model

(Figure 3) has the same mechanics as the rectilinear model and also uses a three dimensional spherical geometry which is more suitable for modeling the brain. This model can provide an adequate understanding of the stress and strain distributions present in the brain during the development of hydrocephalus.

2.2 Marmarou Model

Marmarou et. al., [1] developed the first mathematical model for CSF dynamics that provided some essential insights into the role of ICP in hydrocephalus². In order to avoid some controversies with some terminology used in [1] that have been pointed out in the literature in recent years, there will be no discussion here of some of the physical interpretations of Marmarou's model. The parameters that this model uses are dural sinus pressure, the resistance to CSF absorption and the CSF formation rate. It is important to mention that Marmarou's model has been tested on adult cats and a good agreement has been established between the proposed mathematical model and the measurements [1].

They noticed experimentally that as the fluid was either added or removed from the CSF space, the pressure changed transiently and was followed by a gradual decline back to the initial pressure. This occurs because the CSF volume and pressure are coupled. The rate of CSF formation (I_f) is composed of stored fluid (I_s) and absorbed fluid (I_a); under normal conditions the formation of fluid and the absorption of fluid balance each other so that there is no change in the amount of fluid stored. From this relationship *Marmarou et. al.*, [1] developed a mathematical model for the pressure (P) at time (t) represented by a nonlinear Riccati differential equation of the form:

$$\frac{dP}{dt} - \frac{P^2 K}{R} - PK \left(I_f + \frac{P_d}{R} \right) = 0 \quad (2.2.1)$$

where K is a constant that describes the slope of the pressure-volume curve, R is the resistance to fluid flow, and P_d is the intradural sinus pressure. For an initial condition $P(0) = P_0$, equation (2.2.1) has a solution of the form:

² This section is adapted from [7]

$$P(t) = \frac{\psi(t)}{\frac{1}{P_0} + \frac{K}{R} \int_0^t \psi(\tau) d\tau}, \psi(t) = e^{K \int_0^t I(\tau) d\tau} \quad (2.2.2)$$

Marmarou et. al., [1] investigated three cases that can cause a change in the CSF volume: 1) bolus injection, 2) volume removal, and 3) continuous infusion. For each case $I(t)$ is different and thus different results for $P(t)$ are obtained. The analytic solutions and $I(t)$ for each case are presented in Table 1. The derivations of these equations are given in [7].

Table 1: Analytic Solutions to equation (2.2.1) for the three different cases presented in [1]. Note that is P_t the threshold pressure.

Case	$I(t)$	Analytic Solution
Bolus Injection	$I(t) = I_f + V\delta(t)$	$P(t) = \frac{P_0 e^{KV + Kt(P_0/R)}}{1 + e^{KV} [e^{Kt(P_0/R)} - 1]}$
Volume Removal	$I(t) = I_f - V\delta(t)$	$\begin{cases} P(t) = P_0 e^{K[I_f t - V]}, & \text{if } P(t) < P_t \\ P(t) = \frac{P_0 e^{Kt(P_0/R) - KV}}{1 + e^{-KV} [e^{Kt(P_0/R)} - 1]} \end{cases}$
Continuous Infusion	$I(t) = I_f + \Delta I$	$P(t) = \frac{P_0(P_0 + R\Delta I)}{P_0 + R\Delta I e^{-Kt(P_0 + R\Delta I)/R}}$

Figures 4-6 are plots of the analytic solutions to equation (2.2.2) corresponding to the three cases. In the bolus injection case (Figure 4) some fluid is inserted into the CSF system which adds to the formation rate of CSF. The system was in equilibrium before the fluid was added and was at an initial pressure P_0 . The continuous infusion case (Figure 5) is very similar to the bolus injection case but here the ICP increases rapidly and then stabilizes.

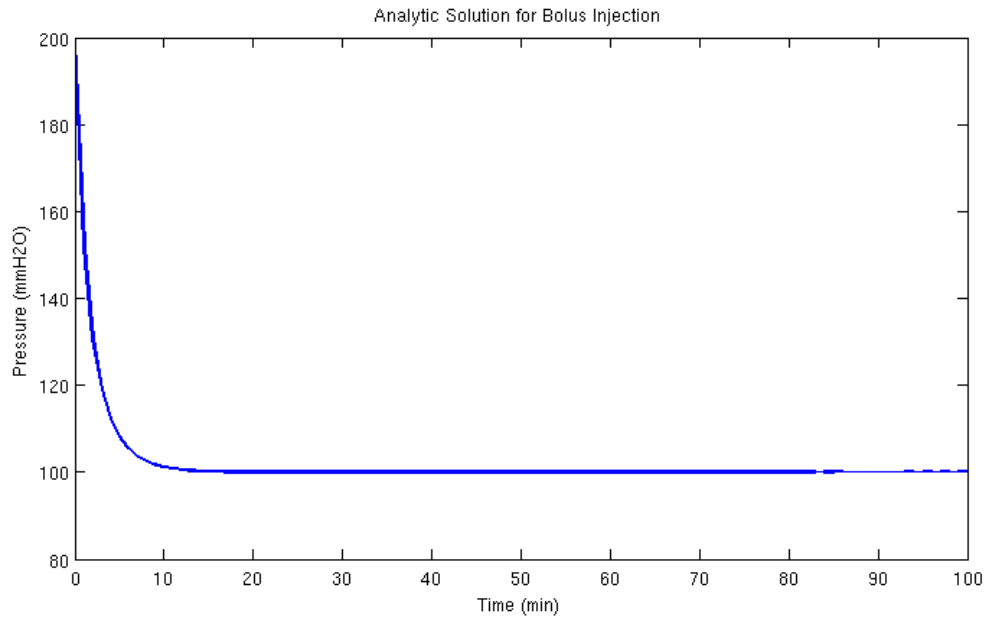


Figure 4: Analytic Solution of Equation (2.2.2) for the bolus injection case.

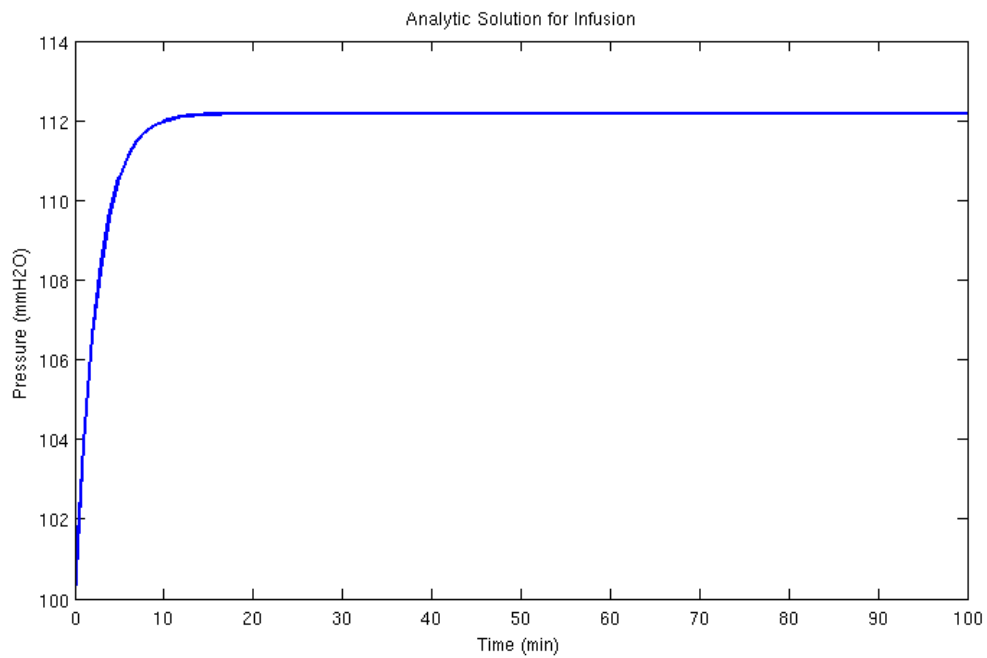


Figure 5: Analytic solution of Equation (2.2.2) for the continuous infusion case.

In the case of volume removal (Figure 6) an additional nonlinearity is introduced when the ICP drops below the given threshold pressure which causes the resistance to absorption to be

increased and leads to a lack of absorption until the pressure meets the threshold pressure again [1]. Once that happens absorption again takes place and the system will return to equilibrium.

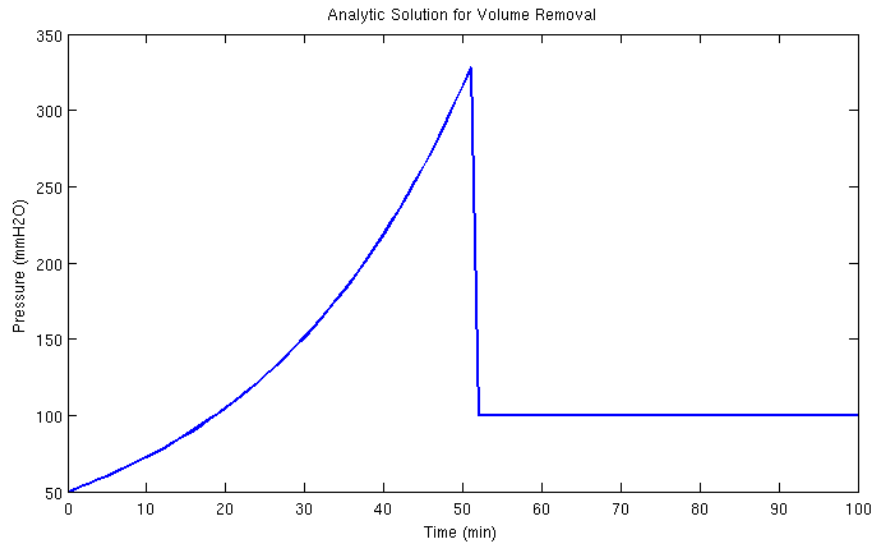


Figure 6: Analytic Solution of Equation (2.2.2) for the case of volume removal.

2.3 Fractional Calculus

Below we will provide some background into the merit in using fractional calculus while modeling the brain. Two models will be described. The first model uses fractional calculus to model neuronal activity whereas the second describes the Hodgkin-Huxley model in terms of fractional derivatives.

2.3.1 Fractional Model for Pyramidal Neurons

In [12] *Lundstorm et. al.* used fractional calculus to describe the firing rate of pyramidal neurons. It was originally thought that neurons followed a single time scale, but upon further investigation *Lundstorm et. al.*, [12] showed that the firing rate of neurons actually depends on the history of the stimulus on that neuron. This implies that multiple time scales are needed to

describe the behavior of neurons, and this can be done using fractional differentiation. It should be noted that fractional differentiation is non-local, so fractional order differentiation is indeed using the history of neuronal activity to calculate the firing rate of the neuron. *Lundstorm et. al.*, [12] discovered that there were a few different mechanisms that could have contributed to the fractional order dynamics that they described. Different geometries of the cells or dendrites, circuit and synaptic mechanisms, and many inactivation states of sodium channels could all contribute to these fractional order dynamics. The use fractional differentiation enhances the responses measured based off of changes in stimulus so that the magnitude and rate of change of the signal is maintained. In addition, it seems that fractional order integration describes the dynamics of muscles and tissue as well as their viscoelastic properties. Tying both fractional order differentiation and integration together leads to *multiple time scales that relate deformations to different biological processes.*

2.3.2 Generalization of Hodgkin-Huxley Model

The Hodgkin-Huxley model uses observations of axons from a giant squid to describe mathematically how action potentials in neurons are initiated and propagated. The model is a system of first order nonlinear ordinary differential equations for sodium activation, potassium activation and leakage. In [13], *Sherief et. al.* generalized the model by replacing the first order temporal derivatives with Caputo fractional order derivatives, described in more detail below. They used the method of Laplace transforms and Mittag-Leffler functions (defined below) to solve their fractional order differential equations. As the fractional order parameters approach unity the solution of those parameters of the generalized model converges to the solution of the classic Hodgkin-Huxley as one would expect.

2.4 Adomian Method

The Adomian method is a very powerful method for solving differential equations. The method builds a series solution analytically to either an ordinary or partial differential equation [14]. The Adomian series tend to converge quickly to the exact solution and therefore the number of terms needed to obtain good approximations is small. It was shown that for simple geometries the Adomian method performs better than classic numerical methods such as finite difference and finite element methods. Recently the method has been extended to solve fractional differential equations. Below we will describe the original Adomian method and then show one of its adaptations for fractional order differential equations which we will use in this thesis.

2.4.1 Classical Adomian Method

The Adomian method takes a differential equation, either partial or ordinary and separates it into a linear part and nonlinear part [14]. The linear part can further be decomposed into an easily invertible part and a remainder. So the differential equation looks like:

$$Lu + Ru + Nu = g \quad (2.4.2)$$

where L is the easily invertible term, R is the remainder of the linear term that is not easily invertible, and N is the nonlinear term as defined by [14]. Once we have our differential equation in this form we want to solve for Lu . Since L is easily invertible, we can take L^{-1} of both sides of Equation (2.4.2). Note that $L^{-1}Lu = u - u(0) - u'(0)t = u - A - Bt$. We look for a solution of the form:

$$u = \sum_{n=0}^{\infty} u_n \quad (2.4.3)$$

which replaced into Equation (2.4.2) gives:

$$\sum_{n=0}^{\infty} u_n = u_0 - L^{-1}R \sum_{n=0}^{\infty} u_n - L^{-1} \sum_{n=0}^{\infty} A_n \quad (2.4.4)$$

where $u_0 = A + Bt + L^{-1}g$, and it is assumed that the nonlinear term was an analytic function of u that can be written as a series expansion of the so-called Adomian polynomials $A_n = \sum_{v=1}^n c(v, n) f^{(v)}(u_0)$ where v is of increasing index, n is the order of the polynomial, and the sum of the subscripts must add to n since A_n is defined in terms of u_0, u_1, \dots, u_n .

The Adomian method has the advantage that we do not have to apply simplifying assumptions where we linearize our equation or subject it to perturbations [14]. A fast converging series solution is more desirable than changing the original problem and having a closed form solution which might be far off from the solution to the original problem.

2.4.2 Fractional Adomian Decomposition Method

Even though fractional order derivatives and integrals have been around since the 17th century, the physical and geometrical interpretations of these fractional order derivatives and integrals has, only recently, been provided by [15] and because of this fractional calculus is now being used for some applications. The most common fractional order derivatives are Riemann-Liouville and Caputo. The Riemann-Liouville integral of order α is defined as:

$$J^\alpha f(x) = \frac{1}{\Gamma(\alpha)} \int_0^x (x-t)^{\alpha-1} f(t) dt \quad \alpha > 0, x > 0 \quad (2.4.5)$$

and it should be noted that [3]:

$$J^\alpha f(x) = \int_{x_0}^x \frac{(x-\xi)^{\alpha-1}}{\Gamma(\alpha)} f(\xi) d\xi = \int_0^{x-x_0} \frac{\xi^{\alpha-1}}{\Gamma(\alpha)} f(x-\xi) d\xi \quad (2.4.6)$$

The definition of the Caputo fractional order derivative tells us to first take ordinary derivatives then a fractional integral:

$$D_*^\alpha f(x) = J^{m-\alpha} \left(\frac{d^m}{dx^m} f(x) \right) \quad m \in \mathbb{N}, \quad m-1 < \alpha < m \quad (2.4.7)$$

On the other hand the definition of the Riemann-Liouville fractional order derivative does the opposite of the Caputo definition, where m and α are identically defined in both cases:

$$D^\alpha f(x) = \frac{d^m}{dx^m} (J^{m-\alpha} f(x)) \quad (2.4.8)$$

Although Caputo derivatives require the functions to be differentiable in the classic sense, they are more desirable because the boundary and initial conditions are included the same way as in classical calculus. On the other hand, Riemann-Liouville derivatives can be applied to non-differentiable functions but special care must be taken when imposing boundary and/or initial conditions due to their non-local nature.

The Adomian solution of a fractional order differential equation like Equation (2.4.2) in which the linear differential operator is replaced by a Caputo fractional derivative is given by the Rach-Adomian-Meyers (RAM) modified decomposition method [3]:

$$u(t) = \sum_{n=0}^{\infty} a_n (t - t_0)^{\alpha n} \quad (2.4.9)$$

where the a_n 's will be expressed below. The Rach-Adomian-Meyers modified decomposition method is the method that we will use below to solve our fractional Marmarou model.

Chapter 3

Fractional Marmarou Model

In this chapter we will develop and solve a fractional Riccati differential equation using the Laplace transform method and the Rach-Adomian-Meyers (RAM) decomposition method. First, we will present the classical equation developed by [1] followed by a presentation of the linear fractional case and then the fractional Riccati equation.

3.1 Classic Marmarou Model

For the sake of completeness we present again Marmarou's model. Marmarou's model [1] is based on the conservation law where the rate for formation of the CSF, I_f , is known and is equal to the sum of the rate of volume change of the CSF stored in the ventricles of the brain, $I_s = \frac{dV}{dt}$, where V is the volume of CSF, and the rate of outflow (absorption) of the CSF, $I_a = \frac{P - P_d}{R}$, where R is the resistance of CSF absorption, P is the pressure of the CSF, and P_d is the pressure of the venous system:

$$I_f = I_s + I_a \quad (3.1.1)$$

or

$$\frac{dV}{dt} = I_f - \frac{P - P_d}{R} \quad (3.1.2)$$

Marmarou introduced the so-called compliance of the CSF system $C = \frac{dV}{dP}$, used the chain rule, $\frac{dV}{dt} = C \frac{dP}{dt}$ and transformed Equation (3.1.2) into:

$$C \frac{dP}{dt} = I_f - \frac{P - P_d}{R} \quad (3.1.3)$$

which is a first order differential equation that is linear in the unknown $P = P(t)$ if $C = C(t)$, and $I_f = I_f(t)$. Now if we assume that $C = \frac{1}{KP}$ where K is a parameter of Marmarou's model, then Equation (3.1.3) becomes a Riccati differential equation of the form:

$$\frac{dP}{dt} + \frac{K}{R}P^2 - K\left(I_f + \frac{P_d}{R}\right)P = 0 \quad (3.1.4)$$

When the initial condition is $P(0) = P_0$, the solution to Equation (3.1.2) is:

$$P(t) = \frac{e^{K \int_0^t I(\tau) d\tau}}{\frac{1}{P_0} + \frac{K}{R} \int_0^t e^{K \int_0^s I(s) ds} d\tau} \quad (3.1.5)$$

where we denote $I(t) = I_f(t) + \frac{P_d}{R}$.

The brain has special properties that provide volume regulation and osmotic pressure that controls CSF flow. In addition, the measurements of CSF pressure are prone to errors due to the complex dynamics of the brain. In order to account not only for the biomechanical behavior of the brain which is still barely known, but also for the uncertainties in CSF pressure measurements in the simplest possible way, we propose to use the fractional Caputo derivative, denoted as ${}_*D_0^\alpha$, of order $0 < \alpha \leq 1$ instead of the first order derivative in Equation (3.1.4). It should be noted that the notation between the Caputo order fractional derivative and the Riemann-Liouville fractional derivative is differentiated by the *. Therefore, we propose the following generalizations to Equations (3.1.3) and (3.1.4):

$$\begin{cases} C \quad {}_*D_0^\alpha P = I_f(t) - \frac{P - P_d}{R} \\ P(0) = P_0 \end{cases} \quad (3.1.6)$$

and respectively if $C = \frac{1}{KP}$:

$$\begin{cases} {}_*D_0^\alpha P + \frac{K}{R}P^2 - K\left(I_f + \frac{P_d}{R}\right)P = 0 \\ P(0) = P_0, \quad 0 < \alpha \leq 1 \end{cases} \quad (3.1.7)$$

Again, in Equations (3.1.6) and (3.1.7) we denote ${}_*D_0^\alpha$ by:

$${}_0^*D_t^\alpha f = \frac{1}{\Gamma(1-\alpha)} \int_0^t \frac{df}{d\tau}(\tau) d\tau = I_0^{1-\alpha} \frac{df}{dt} \quad (3.1.8)$$

the Caputo derivative of order $0 < \alpha \leq 1$. Our fractional models, Equations (3.1.6) and (3.1.7), are based on the assumption that the conservation law of CSF hydrodynamics used in the Marmarou model remains valid when the first order time derivative is replaced by a fractional order derivative. We also notice that although we continue to use the same notations and definitions for the physical quantities and parameters in our models, as in Marmarou's model, they have now different physical units and physical meanings. In our future work we plan to study the physical interpretation of these quantities. Lastly, we point out that our models capture a temporal multiscale effect if we allow $0 < \alpha \leq 1$ to vary.

We will solve Equation (3.1.6) for $C = \frac{1}{K} = \text{constant}$ to gain some insight into the behavior of ${}_0^*D_t^\alpha f$ and then we will solve Equation (3.1.7). Equation (3.1.6) is the fractional linear equation where the solution will be presented in the next section. Equation (3.1.7) is the fractional Riccati differential equation and will be solved in the third section of this chapter.

First we should note that the solution to (3.1.6) when $\alpha = 1$ is the classic solution to a first order linear differential equation:

$$\begin{cases} \frac{dP}{dt} = \frac{-K}{R}P + K \left(I_f + \frac{P_d}{R} \right) \\ P(0) = P_0 \end{cases} \quad (3.1.9)$$

where the solution takes the form:

$$P(t) = P_d + RI_f - (RI_f(0) + P_d - P_0)e^{-tK/R} \quad (3.1.10)$$

Note that here $C = \frac{1}{K}$, and K has different physical units than in [1] where $C = \frac{1}{KP}$. For simplicity we will consider $P_d = P_0$ throughout this thesis.

3.2 Fractional Linear Marmarou Model

Here we present two methods to solve Equation (3.1.6): the Laplace transform method, and the RAM decomposition method (which we will use to solve Equation (3.1.7) as well). Before we do this we should again state that we are aware that the physical meaning of the law in question has been changed, but we will use this model to gain some insight into the behavior of the fractional model proposed. Now let us first consider the Laplace transform method we denote the Laplace transform of f by $\mathcal{L}(f)(s) = \int_0^\infty e^{-st} f(t) dt$. It can be shown that $\mathcal{L}({}_*D_0^\alpha f) = s^\alpha \mathcal{L}(f) - s^{\alpha-1} f(0)$. So, by taking the Laplace transform of Equation (3.1.6), we obtain:

$$s^\alpha \mathcal{L}(P) - s^{\alpha-1} P_0 = K \mathcal{L}(I_f) + \frac{K}{R} P_d \frac{1}{s} - \frac{K}{R} \mathcal{L}(P) \quad (3.2.1)$$

Where the term $\frac{1}{s}$ corresponds to $\mathcal{L}(1)$. We recall that $\mathcal{L}(f * g) = \mathcal{L}(f)\mathcal{L}(g)$ where $f * g = \int_0^t f(t-s)g(s)ds$ is the convolution operation.

We can simplify Equation (3.2.1) to get:

$$\mathcal{L}(P) = \frac{s^{\alpha-1} P_0}{s^\alpha + \frac{K}{R}} + K \frac{\mathcal{L}(I_f)}{s^\alpha + \frac{K}{R}} + \frac{K}{R} P_d \frac{1/s}{s^\alpha + \frac{K}{R}} \quad (3.2.2)$$

Also, from the properties of the Mittag-Leffler function [3, 15], and the generalized Mittag-Leffler function we know that:

$$\begin{cases} E_\alpha(z) = \sum_{k=0}^{\infty} \frac{z^k}{\Gamma(\alpha k + 1)} \\ E_{\alpha,\alpha}(z) = \sum_{k=0}^{\infty} \frac{z^k}{\Gamma(\alpha k + \alpha)} \end{cases}, \quad z \in \mathbb{C}$$

$$\begin{cases} \mathcal{L}(E_\alpha(-\lambda t^\alpha)) = \frac{s^{\alpha-1}}{s^\alpha + \lambda} \\ \mathcal{L}(t^{-(1-\alpha)} E_{\alpha,\alpha}(-\lambda t^\alpha)) = \frac{1}{s^\alpha + \lambda} \end{cases}$$

respectively. Therefore from the above formulas we obtain:

$$\begin{aligned}
P(t) = P_0 E_\alpha \left(-\frac{K}{R} t^\alpha \right) + K \int_0^t \tau^{-(1-\alpha)} E_{\alpha,\alpha} \left(-\frac{K}{R} \tau^\alpha \right) I_f(t-\tau) d\tau \\
+ \frac{K}{R} P_d \int_0^t \tau^{-(1-\alpha)} E_{\alpha,\alpha} \left(-\frac{K}{R} \tau^\alpha \right) d\tau
\end{aligned} \tag{3.2.3}$$

Now we develop the solution from the RAM modified decomposition method proposed by *Duan et. al.*, [3]. The method says that the solution to:

$$\begin{cases}
{}_*\mathcal{D}_{t_0}^\alpha u(t) + \lambda_1 u(t) + \lambda_2 f(u(t)) = g(t), & t_0 < t < T \\
u(t_0) = C_0 \\
u'(t_0) = u''(t_0) = \dots = u^{(m-1)}(t_0)
\end{cases} \tag{3.2.4}$$

where $m - 1 < \alpha \leq m$, is:

$$u(t) = \sum_{n=0}^{\infty} a_n (t - t_0)^{n\alpha} \tag{3.2.5}$$

where

$$\begin{cases}
a_0 = C_0 \\
a_{n+1} = \frac{\Gamma(n\alpha + 1)}{\Gamma(n\alpha + \alpha + 1)} (g_n - \lambda_1 a_n - \lambda_2 A_n), & n = 0, 1, 2, \dots
\end{cases} \tag{3.2.6}$$

with

$$\begin{cases}
g(t) = \sum_{n=0}^{\infty} g_n (t - t_0)^{n\alpha} \\
f(u(t)) = \sum_{n=0}^{\infty} A_n (t - t_0)^{n\alpha} \\
A_n = A_n(a_0, \dots, a_n)
\end{cases} \tag{3.2.7}$$

and the A_n 's are the corresponding Adomian polynomials defined as [3, 14, 15]:

$$\begin{cases}
A_0 = f(u_0) \\
A_1 = u_1 \frac{d}{du_0} f(u_0) \\
A_2 = u_2 \frac{d}{du_0} f(u_0) + \frac{u_1^2}{2!} \frac{d^2}{du_0^2} f(u_0) \\
\dots
\end{cases} \tag{3.2.8}$$

For simplicity we will consider the case of constant infusion of CSF.

$$I_f(t) = \begin{cases} 0, & t < 0 \\ F = \text{constant}, & t \geq 0 \end{cases} \quad (3.2.9)$$

In this case our solution Equation (3.2.3) becomes:

$$P(t) = P_0 E_\alpha \left(-\frac{K}{R} t^\alpha \right) + \int_0^t \left(FK + \frac{K}{R} P_0 \right) \tau^{-(1-\alpha)} E_{\alpha,\alpha} \left(-\frac{K}{R} \tau^\alpha \right) d\tau \quad (3.2.10)$$

based on the Laplace transform method, while the RAM decomposition method give the following solution:

$$P(t) = \sum_{n=0}^{\infty} a_n t^{n\alpha} \quad (3.2.11)$$

where

$$\begin{aligned} a_0 &= P_0 \\ a_1 &= \frac{1}{\Gamma(\alpha + 1)} \left(K \left(F + \frac{P_0}{R} \right) - \frac{K}{R} a_0 \right) \\ a_2 &= \frac{\Gamma(\alpha + 1)}{\Gamma(2\alpha + 1)} \left(-\frac{K}{R} a_1 \right) \\ a_3 &= \frac{\Gamma(2\alpha + 1)}{\Gamma(3\alpha + 1)} \left(-\frac{K}{R} a_2 \right) \end{aligned} \quad (3.2.12)$$

etc.

Plugging in the coefficients in Equation (3.2.12) into Equation (3.2.11) and comparing the results to Equation (3.2.10) it can be shown the solutions do agree as they should. Therefore, both the Laplace transform method and the RAM modified decomposition method give the same results. This validates the RAM decomposition method which we will use further to solve Equation (3.1.7).

3.3 Fractional Nonlinear Marmarou Model

In this section we will develop solutions to Equation (3.1.7). For this differential equation we will consider the three different cases that are presented in [1]: bolus injection, volume removal, and continuous infusion. Bolus injection and volume removal differ only by a sign so they will be solved together using the \pm operator to distinguish between the two. Note that bolus injection corresponds to the plus and volume removal corresponds to the minus. We will start by first considering bolus injection/volume removal and then move on to continuous infusion at the end of this section.

3.3.1 Bolus Injection/Volume Removal

For the case of bolus injection/volume removal $I_f = F \pm V\delta(t)$. Since the case of constant infusion (discussed below) accounts for the constant term in I_f we can restrict the cases of bolus injection/volume removal to just the term described by the Dirac delta function because a linear superposition of the solutions in the constant infusion case and either in the bolus injection or in the volume removal case will get us back to the original definition described in [1]. So without loss of generality we will consider the case when $I_f(t) = \pm V\delta(t)$. For these two cases the solutions proposed by Marmarou are not valid. As we have mentioned in Chapter 2, *Marmarou et. al.*, [1] used the integration factor method to solve Equation (3.1.4), but this method does not work under the case when $I_f = \pm V\delta(t)$ because the Dirac delta function is not continuous. Also, it should be noted that at short time scales Marmarou's solutions for these two cases do not satisfy the initial conditions proposed by *Marmarou et. al.*, [1]. To develop a valid solution we must use a continuous approximation of the Dirac delta function. We choose $\delta(t) = \lim_{\varepsilon \rightarrow 0} \frac{1}{2} \varepsilon |t|^{\varepsilon-1}$, where the function $\delta_\varepsilon(t) = \frac{1}{2} \varepsilon |t|^{\varepsilon-1}$ is continuous $\forall \varepsilon > 0, \varepsilon \rightarrow 0$. Thus

for the cases of bolus injection and volume removal we can solve Equation (3.1.4) for $I_f = \pm V \delta_\varepsilon(t)$ using the integrating factor method and so we get from Equation (3.1.5):

$$P_\varepsilon(t) = \frac{e^{K \int_0^t (\pm \frac{1}{2} V \varepsilon s^{\varepsilon-1} + P_0/R) ds}}{P_0 + \frac{K}{R} \int_0^t e^{K \int_0^\tau (\pm \frac{1}{2} V \varepsilon s^{\varepsilon-1} + P_0/R) ds} d\tau}$$

or equivalently:

$$P_\varepsilon(t) = \frac{e^{K(\pm \frac{1}{2} V t^\varepsilon + \frac{P_0}{R} t)}}{\frac{1}{P_0} + \frac{K}{R} \int_0^t e^{K(\pm \frac{1}{2} V \tau^\varepsilon + \frac{P_0}{R} \tau)} d\tau} \quad (3.3.1)$$

The integral in Equation (3.3.1) are evaluated numerically. Then the solution is:

$$P(t) = \lim_{\varepsilon \rightarrow 0} P_\varepsilon(t)$$

To solve Equation (3.1.7) we will again use the RAM decomposition method outlined in [3] and Equation (3.2.4) – (3.2.8), and the fractional Taylor series representation of a function expressed with the help of the Caputo fractional derivatives of order $0 < \alpha \leq 1$ [16]:

$$g(t) = \sum_{j=0}^{\infty} \frac{(t-t_0)^{j\alpha}}{\Gamma(j\alpha+1)} {}_t_0^{j\alpha} g(t_{0+}) \quad (3.3.2)$$

where ${}_t_0^{j\alpha} g = {}_t_0^\alpha {}_t_0^\alpha \dots {}_t_0^\alpha g \neq {}_t_0^{\alpha+\alpha+\dots+\alpha} g$, where ${}_t_0^\alpha$ on the left side, and α on the right side are repeated j times. We can use Equation (3.3.2) to find the needed coefficients g_n in Equation (3.2.7).

We propose now a small generalization to the theory presented in [3], namely we want to use the RAM modified decomposition method to solve the following variation to Equation (3.2.4):

$$\begin{cases} {}_t_0^\alpha u(t) + \lambda_1 u(t) + \lambda_2 h(t)u(t) + \lambda_3 f(u(t)) = g(t), & 0 < \alpha \leq 1 \\ u(t_0) = C_0 \end{cases} \quad (3.3.3)$$

since our Equation (3.1.7) is in fact of the same form as Equation (3.3.3). Using Equation (3.3.2)

we can write the fractional Taylor series for h, g as:

$$h(t) = \sum_{n=0}^{\infty} h_n(t-t_0)^{n\alpha}, \quad g(t) = \sum_{n=0}^{\infty} g_n(t-t_0)^{n\alpha} \quad (3.3.4)$$

We can look for a solution to Equation (3.3.3) of the form of Equation (3.2.5). We substitute

Equations (3.2.5), (3.2.7), and (3.3.4) into Equation (3.3.3) and get:

$$\begin{aligned} & \sum_{n=0}^{\infty} a_n {}_t_0^{\alpha} D^{\alpha}((t-t_0)^{n\alpha}) + \sum_{n=0}^{\infty} \lambda_1 a_n (t-t_0)^{n\alpha} + \sum_{n=0}^{\infty} \lambda_2 \left(\sum_{k=0}^n a_k h_{n-k}(t-t_0)^{n\alpha} \right) \\ & + \sum_{n=0}^{\infty} \lambda_3 A_n (t-t_0)^{n\alpha} = \sum_{n=0}^{\infty} g_n (t-t_0)^{n\alpha} \end{aligned} \quad (3.3.5)$$

Since ${}_t_0^{\alpha} D^{\alpha}((t-t_0)^{n\alpha}) = \frac{\Gamma(n\alpha+1)}{\Gamma(n\alpha-\alpha+1)}(t-t_0)^{(n-1)\alpha}$ Equation (3.3.5) becomes:

$$\begin{aligned} & \frac{a_0}{\Gamma(1-\alpha)}(t-t_0)^{-\alpha} \\ & + \sum_{n=0}^{\infty} \left[a_{n+1} \frac{\Gamma((n+1)\alpha+1)}{\Gamma(n\alpha+1)} + \lambda_1 a_n + \lambda_2 \sum_{k=0}^n a_k h_{n-k} + \lambda_3 A_n - g_n \right] (t-t_0)^{n\alpha} = 0 \end{aligned} \quad (3.3.6)$$

and therefore:

$$\begin{cases} a_0 = u(t_0) = C_0 \\ a_{n+1} = \frac{\Gamma(n\alpha+1)}{\Gamma((n+1)\alpha+1)} \left(g_n - \lambda_1 a_n - \lambda_3 A_n - \sum_{k=0}^n \lambda_2 a_k h_{n-k} \right) \end{cases} \quad (3.3.7)$$

where $n = 0, 1, 2, \dots$

We notice that the sum in Equation (3.2.5) does not converge everywhere; the radius of convergence is given by [3]:

$$\rho_n(\alpha) = \left(\frac{1}{\sqrt[n]{|a_n|}} \right)^{1/\alpha}$$

We can now return to our fractional Marmarou's model, Equation (3.1.7). We look for a solution of the form shown in Equation (3.2.5). For the cases of bolus injection and volume removal we let

$I_f = \pm V\delta(t) = \tilde{V}\delta(t)$, take $\delta(t) = \lim_{\varepsilon \rightarrow 0} \frac{1}{2\sqrt{\pi\varepsilon}} e^{-t^2/(4\varepsilon)}$ (this choice makes the calculations simpler) and solve:

$$\begin{cases} {}_0^*D_0^\alpha P_\varepsilon + \frac{K}{R} P_\varepsilon^2 - K \left(\tilde{V} \frac{1}{2\sqrt{\pi\varepsilon}} e^{-t^2/(4\varepsilon)} + \frac{P_0}{R} \right) P_\varepsilon = 0 \\ P_\varepsilon(0) = P_0 \end{cases} \quad (3.3.8)$$

Thus for the cases of bolus injection and volume removal $P(t) = \lim_{\varepsilon \rightarrow 0} P_\varepsilon(t)$ where P_ε is the solution to Equation (3.3.8).

Since Equation (3.1.7) is of the form of Equation (3.3.3) we get from the formulas presented above that:

$$P_\varepsilon(t) = \sum_{n=0}^{\infty} a_n t^{n\alpha}$$

with

$$\begin{cases} a_0 = P_0 \\ a_{n+1} = \frac{\Gamma(n\alpha + 1)}{\Gamma(n\alpha + \alpha + 1)} \left(\frac{KP_0}{R} a_n - \frac{K}{R} A_n + K\tilde{V} \sum_{j=0}^n a_j h_{n-j} \right), \quad n = 0, 1, 2, \dots \\ \begin{cases} A_0 = a_0^2 \\ A_1 = 2a_0 a_1 \\ A_2 = a_1^2 + 2a_0 a_2 \\ \dots \end{cases} \end{cases}$$

where the Adomian polynomials correspond to $f(P) = P^2$. We also have that:

$$h(t) = \sum_{j=0}^{\infty} \frac{t^{j\alpha}}{\Gamma(j\alpha + 1)} {}_0^*D_0^{j\alpha} h(0_+) \equiv \frac{1}{2\sqrt{\pi\varepsilon}} e^{-t^2/(4\varepsilon)}$$

with

$${}_0^*D_0^\alpha h(0_+) = \frac{1}{\Gamma(1-\alpha)} \lim_{t \rightarrow 0} \int_0^t \frac{dh(s)}{(t-s)^\alpha} ds$$

We denote by $h_j = \frac{{}_*D_0^{j\alpha} h(0_+)}{\Gamma(j\alpha+1)}$ and these are some of the parameters needed to calculate a_n above.

Therefore:

$$P_\varepsilon = a_0 + a_1 t^\alpha + a_2 t^{2\alpha} + \dots \quad (3.3.9)$$

with

$$\begin{aligned} a_0 &= P_0 \\ a_1 &= \frac{K\tilde{V}P_0}{\Gamma(\alpha+1)} \\ a_2 &= \frac{K\tilde{V}P_0}{\Gamma(2\alpha+1)} \left(K\tilde{V} - \frac{KP_0}{R} + \Gamma(\alpha+1)h_1 \right) \end{aligned} \quad (3.3.10)$$

a_1 has this form since $h_0 = 1$ and in a_2 we have that:

$$h_1 = \frac{1}{\Gamma(\alpha+1)\Gamma(1-\alpha)} \lim_{\substack{t \rightarrow 0 \\ \varepsilon \rightarrow 0}} \frac{-1}{4\sqrt{\pi\varepsilon^3}} \int_0^t \frac{s e^{-s^2/(4\varepsilon)}}{(t-s)^\alpha}$$

3.3.2 Continuous Infusion

In this case we use directly the RAM decomposition method to solve Equation (3.1.7).

We denote by:

$$\begin{cases} \beta_1 = -K \left(F + \frac{P_d}{R} \right) = \text{constant} \\ \beta_2 = \frac{K}{R} = \text{constant} \end{cases} \quad (3.3.11)$$

and rewrite Equation (3.1.7) as:

$$\begin{cases} {}_*D_0^\alpha P + \beta_1 P + \beta_2 P^2 = 0 \\ P(0) = P_0 \end{cases} \quad (3.3.12)$$

whose solution is according to Equation (3.2.5) of the form:

$$P(t) = \sum_{n=0}^{\infty} a_n t^{n\alpha} \quad (3.3.13)$$

where

$$a_0 = P_0$$

$$a_{n+1} = \frac{\Gamma(n\alpha + 1)}{\Gamma(n\alpha + \alpha + 1)} (-\beta_1 a_n - \beta_2 A_n), n = 0, 1, 2 \dots$$

with Adomian polynomials:

$$A_0 = a_0^2$$

$$A_1 = 2a_0 a_1$$

$$A_2 = a_1^2 + 2a_0 a_2$$

...

$$A_n = \sum_{k=0}^n a_{n-k} a_k$$

3.4 Results

For our numerical simulations we used the following parameters that were found experimentally by [1] while they were investigating possible mechanisms for the onset of hydrocephalus in adult cats: $P_0 = P_d = 100[\text{mmH}_2\text{O}]$, $K = 1/0.4343 [\text{mL}^{-1}\text{min}^{-\alpha}]$, $R = 609[\text{mmH}_2\text{O}\text{mL}^{-1}\text{min}]$, $V_0 = 3[\text{mL}]$, a constant rate of infusion $F = 0.02[\text{mLmin}^{-1}]$ in the constant infusion case, and $V = 0.02[\text{mL}]$ in bolus injection. Note that we are not showing any results from the case of volume removal since it is similar to the the case of bolus injection. Given that the duration of the experiments in [1] were on the order of six to eight minutes, and that the radii of convergence of our series solutions impose limitations we will show our results

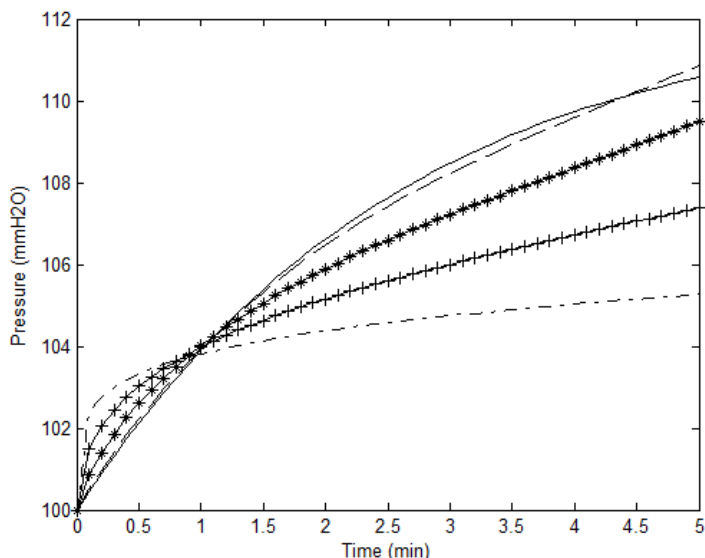


Figure 7: Shape of CSF pressure for the case of constant infusion for the following values of α : 0.25(-), 0.5 (+), 0.75 (*), 0.95 (-). The solid line corresponds to the solution given by Equation (3.1.5).

can see that as α goes to 1 the pressures tend to converge to the pressure given by Equation (3.1.5). Also, the initial slope of the CSF pressure decreases as α increases. We hypothesize that during slow development of hydrocephalus when the CSF accumulates in the ventricles due to a constant CSF infusion, and the CSF pressure increases abruptly initially and then its increase slows down possibly due to controllers like special proteins in the brain that provide volume

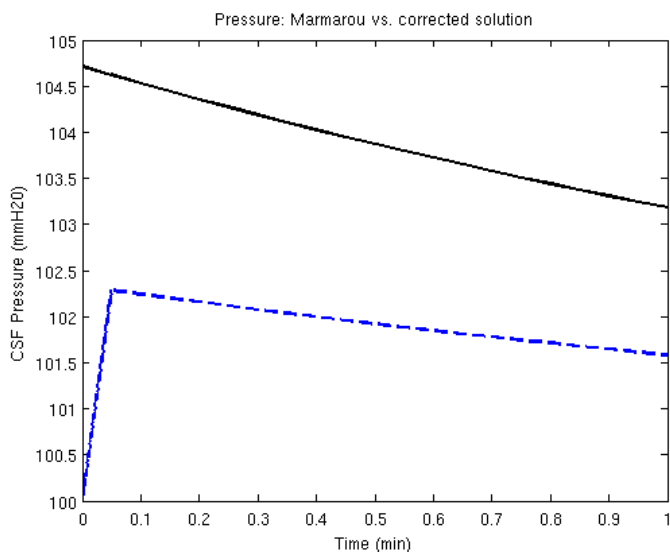


Figure 8: In the case of bolus injection, the CSF pressure found in [1] is shown as a solid line, while the dashed blue line shows the CSF pressure calculated using a sequence of continuous functions to approximate the Dirac distribution.

for a time period of five minutes for the case of constant infusion and for a period of up to one minute for the case of bolus injection. Figure 7 shows the solutions to Equation (3.3.11) for different values of $\alpha < 1$ and the solution to Equation (3.1.5) for $\alpha = 1$. We

regulation and osmotic pressures. In this context the shapes of the CSF pressure for $\alpha < 0.5$ shown in Figure 7 capture our interpretation of the CSF-brain interactions.

Figure 8 shows the corrected CSF pressure for the

case of bolus injection (dashed blue line) using an approximation for the Dirac distribution which is then compared to the original solution proposed by [1]. The two solutions do not agree on short times, which was expected, although at longer times the two solutions will eventually coincide. In Figure 9a and 9b we show the temporal variations of the CSF pressure as given by Equations (3.3.9) and (3.3.10). While the initial slope of the pressure decreases as α approaches 1, the pressure given by Equations (3.3.9) and (3.3.10) does not converge to the CSF pressure calculated using an approximation of the Dirac distribution (Figure 9b).

In our future work we plan to add more terms to Equation (3.3.9) as well as use Padé Approximates as in [3] to get the expected convergence as α goes to 1. We will also implement better numerical solvers for the coefficients of $h_n, n = 0,1,2 \dots$ of the fractional Taylor series of $h(t)$ needed in Equation (3.3.10). We should note that if after all of these improvements we still see the same asymptotic behavior of the CSF pressure for $\alpha < 0.5$ (Figure 9a) we could hypothesize that at later times the CSF volume may increase and then it could model the slow development of hydrocephalus. This means that bolus injection of CSF could in fact cause hydrocephalus when the CSF-brain dynamics has been somehow compromised³. Thus, our fractional pressure-volume model appears to capture certain processes happening at time scales of order $\alpha < 0.5$ which could cause the onset of hydrocephalus either by constant infusion of CSF or by CSF bolus injection. A constant infusion CSF is by now a known and accepted mechanism for hydrocephalus; however, the bolus injection is a new and rather unexpected cause of hydrocephalus. A deeper and more thorough analysis of our model along with experiments is needed in order to consider this as plausible.

³ We suspect that in hydrocephalus the CSF is a non-Newtonian fluid (while in healthy subjects it is already known that the CSF is Newtonian). Dr. Steven Schiff, Private communication.

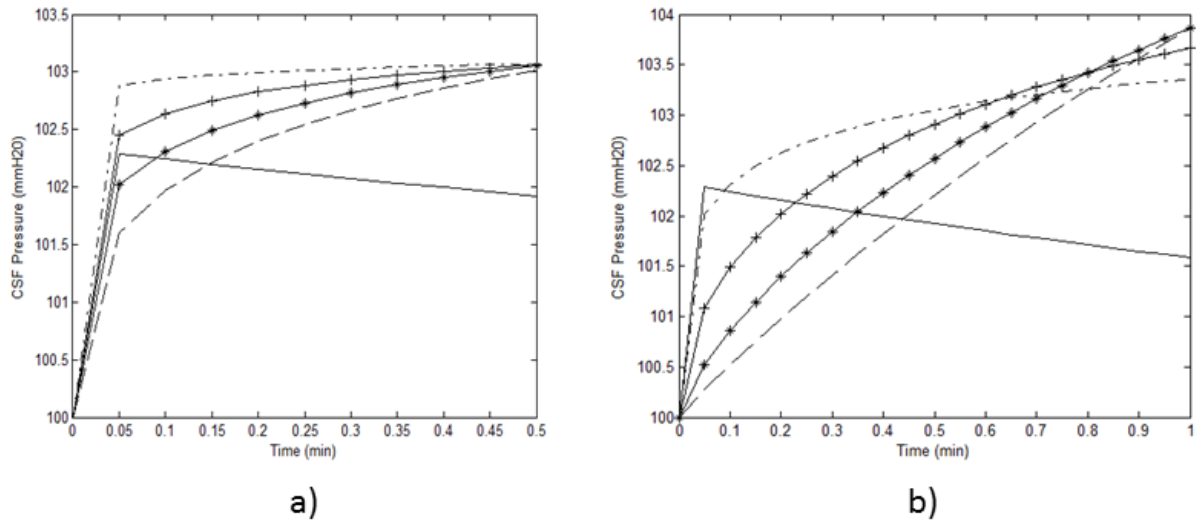


Figure 9: The shapes of the CSF pressure for the case of bolus injection for the following values of α : a) 0.05 (-), 0.15(+), 0.25 (*), 0.35 (-). The solid line shows our approximate solutions to Marmarou's model in this case. The largest radius of convergence corresponds to $\alpha = 0.35$ and is given by $\rho_2 = 0.4754$, and b) 0.25 (-), 0.5 (+), 0.75 (*), 0.95 (-). The solid line shows our approximate solutions to Marmarou's model in this case. The largest radius of convergence corresponds to $\alpha = 0.95$ and is given by $\rho_2 = 1.0983$.

3.5 Concluding Remarks

Before moving to the next chapter, we would like to mention another possible generalization of Marmarou's model using the left Riemann-Liouville fractional order derivative.

We start by defining some "averaged" values of the CSF volume and pressure as:

$$\begin{cases} \mathcal{V}(t) = I_0^{1-\alpha} V(t) = \frac{1}{\Gamma(1-\alpha)} \int_0^t \frac{V(\tau) d\tau}{(t-\tau)^\alpha} \\ \mathcal{P}(t) = I_0^{1-\alpha} P(t) = \frac{1}{\Gamma(1-\alpha)} \int_0^t \frac{P(\tau) d\tau}{(t-\tau)^\alpha} \end{cases}, \quad 0 < \alpha \leq 1 \quad (3.5.1)$$

These new quantities $\mathcal{V}(t)$ and $\mathcal{P}(t)$ are multiscaled volume and pressure in time because of the fractional order integral, $I_0^{1-\alpha}$. Thus, from a practical point of view, these quantities should be less sensitive to inherent measurement errors than $V(t)$ and $P(t)$.

Marmarou's conservation law Equation (3.1.2) becomes in this case:

$$\frac{dV}{dt} = I_f - \frac{P - P_d}{R} \quad (3.5.2)$$

and C becomes $C = \frac{dV}{dP}$ so that Equation (3.5.2) becomes:

$$C \frac{dP}{dt} = I_f - \frac{P - P_d}{R}$$

or equivalently:

$$CD_0^\alpha P = I_f - \frac{P - P_d}{R} \quad (3.5.3)$$

Where $D_0^\alpha P = \frac{1}{\Gamma(1-\alpha)} \frac{d}{dt} \int_0^t \frac{P(\tau) d\tau}{(t-\tau)^\alpha} = \frac{d}{dt} I_0^{1-\alpha} P$ is the left-sided Riemann-Liouville fractional order derivative of order $0 < \alpha \leq 1$. With Equation (3.5.3) we have the following non-local initial condition:

$$I_0^{1-\alpha} P(0_+) = P_0 \quad (3.5.4)$$

As before we will consider the following initial value problems:

$$\begin{cases} D_0^\alpha P = -\frac{K}{R} P + K \left(I_f + \frac{P_d}{R} \right), & 0 < \alpha \leq 1 \\ I_0^{1-\alpha} P(0_+) = P_0 \end{cases} \quad (3.5.5)$$

the fractional linear case and:

$$\begin{cases} D_0^\alpha P + \frac{K}{R} P^2 - K \left(I_f + \frac{P_d}{R} \right) P = 0, & 0 < \alpha \leq 1 \\ I_0^{1-\alpha} P(0_+) = P_0 \end{cases} \quad (3.5.6)$$

the fractional Riccati case. For the case of constant infusion of CSF we have that K , R , and $I_f = f = \text{constant}$ are all constants and as before we assume $P_d = P_0$.

To solve Equation (3.5.5) we use the Laplace transform method. By applying the Laplace transform to Equation (3.5.5) we get:

$$s^\alpha \mathcal{L}(P) - I_0^{1-\alpha} P(0_+) = -\frac{K}{R} \mathcal{L}(P) + K \mathcal{L}(I_f) + \frac{P_0 K}{R} \mathcal{L}(1)$$

and since $\mathcal{L}(1) = 1/s$, $\mathcal{L}(I_f) = F\mathcal{L}(1)$, and $I_0^{1-\alpha}P(0_+) = P_0$ the above equation simplifies to:

$$\left(s^\alpha + \frac{K}{R}\right)\mathcal{L}(P) = P_0 + K\left(F + \frac{P_0}{R}\right)\frac{1}{s}$$

Now recalling that $\mathcal{L}\left(t^{-(1-\alpha)}E_{\alpha,\alpha}(-\lambda t^\alpha)\right) = \frac{1}{s^\alpha + \lambda}$ and $\mathcal{L}\left(\int_0^t f(\tau)d\tau\right) = \frac{1}{s}\mathcal{L}(f)$ we get that the solution to Equation (3.5.5) of the form:

$$P(t) = P_0 t^{-(1-\alpha)}E_{\alpha,\alpha}\left(-\frac{K}{R}t^\alpha\right) + K\left(F + \frac{P_0}{R}\right)\int_0^t \tau^{-(1-\alpha)}E_{\alpha,\alpha}\left(-\frac{K}{R}\tau^\alpha\right)d\tau \quad (3.5.7)$$

To solve Equation (3.5.6) we use the RAM decomposition method and look for a solution of the form $P = \sum_{n=0}^{\infty} \tilde{P}_n$ with $I_0^{1-\alpha}\tilde{P}_0 = P_0$ and $P^2 = \sum_{n=0}^{\infty} A_n$, where A_n 's are the same Adomain polynomials we used to solve the fractional Riccati differential equation with the Caputo fractional derivative. Let $L = \frac{d}{dt}$ and $L^{-1} = \int_0^t$ be operators. We then have:

$$L^{-1}|D_0^\alpha P = \frac{d}{dt}I_0^{1-\alpha}P = K\left(F + \frac{P_0}{R}\right)P - \frac{K}{R}P^2$$

such that:

$$I_0^{1-\alpha}P - P_0 = K\left(F + \frac{P_0}{R}\right)L^{-1}P - \frac{K}{R}L^{-1}(P^2)$$

which we can further written as:

$$I_0^{1-\alpha}\left(\sum_{n=0}^{\infty} \tilde{P}_n\right) = P_0 + K\left(F + \frac{P_0}{R}\right)L^{-1}\left(\sum_{n=0}^{\infty} \tilde{P}_n\right) - \frac{K}{R}L^{-1}(P^2)$$

with

$$\left\{ \begin{array}{l} I_0^{1-\alpha}\tilde{P}_0 = P_0 \\ I_0^{1-\alpha}\tilde{P}_1 = K\left(F + \frac{P_0}{R}\right)L^{-1}\tilde{P}_0 - \frac{K}{R}L^{-1}(A_0(P^2)) \\ I_0^{1-\alpha}\tilde{P}_2 = K\left(F + \frac{P_0}{R}\right)L^{-1}\tilde{P}_1 - \frac{K}{R}L^{-1}(A_1(P^2)) \\ \dots \\ I_0^{1-\alpha}\tilde{P}_n = K\left(F + \frac{P_0}{R}\right)L^{-1}\tilde{P}_{n-1} - \frac{K}{R}L^{-1}(A_{n-1}(P^2)) \end{array} \right.$$

Whereas before

$$A_0 = \tilde{P}_0^2$$

$$A_1 = 2\tilde{P}_0\tilde{P}_1$$

$$A_2 = \tilde{P}_1^2 + 2\tilde{P}_0\tilde{P}_2$$

$$A_3 = 2\tilde{P}_1\tilde{P}_2 + 2\tilde{P}_0\tilde{P}_3$$

$$A_4 = \tilde{P}_2^2 + 2\tilde{P}_1\tilde{P}_3 + 2\tilde{P}_0\tilde{P}_4$$

$$A_5 = 2\tilde{P}_2\tilde{P}_3 + 2\tilde{P}_1\tilde{P}_4 + 2\tilde{P}_0\tilde{P}_5$$

...

It is known that the following inversion formula is true for the left-sided Riemann-Liouville derivative and the Riemann-Liouville integral:

$$D_0^\alpha I_0^\alpha f = f$$

Thus if we want to solve $I_0^{1-\alpha}\tilde{P}_0 = P_0$ for \tilde{P}_0 for the unknown \tilde{P}_0 we just need to:

$$D_0^{1-\alpha} I_0^{1-\alpha} \tilde{P}_0 = D_0^{1-\alpha} P_0$$

Which gives:

$$\tilde{P}_0 = P_0 D_0^{1-\alpha}(1) = P_0 \frac{t^{-1+\alpha}}{\Gamma(\alpha)}$$

and so

$$A_0 = \left(\frac{P_0}{\Gamma(\alpha)}\right)^2 t^{-2+2\alpha}$$

Next, we need to solve the following for \tilde{P}_1 :

$$D_0^{1-\alpha} | I_0^{1-\alpha} \tilde{P}_1 = K \left(F + \frac{P_0}{R}\right) \int_0^t \frac{P_0}{\Gamma(\alpha)} \tau^{-1+\alpha} d\tau - \frac{K}{R} \int_0^t \left(\frac{P_0}{\Gamma(\alpha)}\right)^2 \tau^{-2+2\alpha} d\tau$$

which evaluates to:

$$D_0^{1-\alpha} | I_0^{1-\alpha} \tilde{P}_1 = \frac{P_0 K}{\Gamma(\alpha)} \left(F + \frac{P_0}{R}\right) \frac{t^\alpha}{\alpha} - \frac{P_0^2 K}{\Gamma(\alpha)^2 R} \frac{t^{2\alpha-1}}{2\alpha-1}$$

Therefore:

$$\tilde{P}_1 = \frac{P_0 K}{\alpha \Gamma(\alpha)} \left(F + \frac{P_0}{R} \right) D_0^{1-\alpha} t^\alpha - \frac{P_0^2 K}{(2\alpha - 1) \Gamma(\alpha)^2 R} D_0^{1-\alpha} t^{2\alpha-1}$$

It is known that:

$$D_0^\alpha t^\eta = \frac{\Gamma(\eta + 1)}{\Gamma(\eta + 1 - \alpha)} t^{\eta-\alpha}, \quad \alpha > 0, \eta > -1, t > 0$$

and therefore:

$$D_0^{1-\alpha} t^\alpha = \frac{\Gamma(\alpha + 1)}{\Gamma(\alpha + 1 - 1 + \alpha)} t^{\alpha-(1-\alpha)} = \frac{\Gamma(\alpha + 1)}{\Gamma(2\alpha)} t^{2\alpha-1}$$

$$D_0^{1-\alpha} t^{2\alpha-1} = \frac{\Gamma(2\alpha)}{\Gamma(2\alpha - 1 + 1 - 1 + \alpha)} t^{2\alpha-1-(1-\alpha)} = \frac{\Gamma(2\alpha)}{\Gamma(3\alpha - 1)} t^{3\alpha-2}$$

We finally get:

$$\tilde{P}_1 = P_0 K \left(F + \frac{P_0}{R} \right) \frac{\Gamma(\alpha + 1)}{\alpha \Gamma(\alpha) \Gamma(2\alpha)} t^{2\alpha-1} - \frac{P_0^2 K}{R} \frac{\Gamma(2\alpha)}{(2\alpha - 1) \Gamma(\alpha)^2 \Gamma(3\alpha - 1)} t^{3\alpha-2}$$

and

$$A_1 = 2 \frac{P_0}{\Gamma(\alpha)} t^{\alpha-1} \left[P_0 K \left(F + \frac{P_0}{R} \right) \frac{\Gamma(\alpha + 1)}{\alpha \Gamma(\alpha) \Gamma(2\alpha)} t^{2\alpha-1} - \frac{P_0^2 K}{R} \frac{\Gamma(2\alpha)}{(2\alpha - 1) \Gamma(\alpha)^2 \Gamma(3\alpha - 1)} t^{3\alpha-2} \right]$$

We follow the same procedure for \tilde{P}_2 and end up with:

$$\tilde{P}_2 = P_0 K^2 \left(F + \frac{P_0}{R} \right)^2 \frac{\Gamma(\alpha+1)\Gamma(2\alpha+1)}{2\alpha^2\Gamma(\alpha)\Gamma(2\alpha)\Gamma(3\alpha)} t^{3\alpha-1} - \frac{P_0^2 K^2}{R} \frac{\Gamma(2\alpha)\Gamma(3\alpha+2)}{(2\alpha-1)(3\alpha+1)\Gamma(\alpha)^2\Gamma(3\alpha-1)\Gamma(4\alpha+1)} t^{4\alpha} +$$

$$2 \frac{P_0^2 K^2}{R^2} \left(F + \frac{P_0}{R} \right) \frac{\Gamma(\alpha+1)\Gamma(3\alpha)}{\alpha(3\alpha+1)\Gamma(\alpha)^2\Gamma(2\alpha)\Gamma(4\alpha-1)} t^{4\alpha-2} + 2 \frac{P_0^3 K^2}{R^2} \frac{\Gamma(2\alpha)\Gamma(4\alpha+1)}{\alpha(2\alpha-1)\Gamma(\alpha)^3\Gamma(3\alpha-1)\Gamma(5\alpha)} t^{5\alpha-1}$$

And now A_2 can now be calculated. Therefore the solution to Equation (3.5.6) is:

$$P \approx \tilde{P}_0 + \tilde{P}_1 + \tilde{P}_2 \quad (3.5.8)$$

In most cases the Adomian series converges to the solution of a given initial (or boundary) value problem in four to six terms. We note that we could calculate more terms through symbolic computations on a computer. Also, for $\alpha = 1$ Equation (3.5.8) should be the

McLaurin series of the classic Riccati differential equation proposed by *Marmarou et. al.*, [1]. In our further work we intend to solve Equations (3.5.5) and (3.5.6) for the cases of bolus injection/volume removal and compare the results obtained for the Riemann-Liouville fractional and the Caputo fractional Riccati differential equations.

Chapter 4

Stress Strain Analysis in a Cylindrical Geometry with Applications to Brain-CSF Interactions

In this chapter we investigate the effects of the behavior of CSF dynamics on brain tissue. For simplicity we use a cylindrical geometry of the brain and the CSF dynamics is described by either Marmarou's model or by our (Caputo) fractional Marmarou model.

4.1 Theory

We present first a classic two-dimensional problem in elasto-statics⁴ [17]. We denote by

$$\sigma = \begin{pmatrix} \sigma_x & \tau_{xy} & 0 \\ \tau_{xy} & \sigma_y & 0 \\ 0 & 0 & 0 \end{pmatrix} \quad (4.1)$$

a plane stress field acting on a body where weight is the only force. We assume that the density is uniform in the body, $\rho = \text{constant}$. The equilibrium equations are in this case:

$$\begin{cases} \frac{\partial}{\partial x} \sigma_x + \frac{\partial}{\partial y} \tau_{xy} = 0 \\ \frac{\partial}{\partial x} \tau_{xy} + \frac{\partial}{\partial y} \sigma_y + \rho g = 0 \end{cases} \quad (4.2)$$

where we need to solve for σ_x , σ_y , and τ_{xy} so that they will satisfy the boundary conditions. System (4.2) is indeterminate because we have three unknowns, and only two equations. To get this third equation we must use the condition of compatibility of strains so that we can guarantee the existence of the displacement components, u and v . For infinitesimal deformations in plane, the strain components are:

⁴ This chapter is adapted from [7]

$$\varepsilon_x = \frac{\partial u}{\partial x}, \varepsilon_y = \frac{\partial v}{\partial y}, \gamma_{xy} = \frac{\partial u}{\partial y} + \frac{\partial v}{\partial x} \quad (4.3)$$

It can be shown that the condition of integrability for (4.3) is:

$$\frac{\partial^2 \varepsilon_x}{\partial y^2} + \frac{\partial^2 \varepsilon_y}{\partial x^2} = \frac{\partial^2 \gamma_{xy}}{\partial x \partial y} \quad (4.4)$$

which is also known as the condition of compatibility for admissible strains.

We further assume that the body is made of an isotropic linear elastic material, and therefore the inverse form of Hooke's Law is:

$$\begin{cases} \varepsilon_x = \frac{1}{E}(\sigma_x - \nu\sigma_y) \\ \varepsilon_y = \frac{1}{E}(\sigma_y - \nu\sigma_x) \\ \gamma_{xy} = \frac{2(1+\nu)}{E}\tau_{xy} \end{cases} \quad (4.5)$$

with E being Young's modulus and ν Poisson's ratio. By replacing (4.5) into (4.3) the expression in the stresses of the condition of compatibility is:

$$\frac{\partial^2}{\partial y^2}(\sigma_x - \nu\sigma_y) + \frac{\partial^2}{\partial x^2}(\sigma_y - \nu\sigma_x) = 2(1+\nu)\frac{\partial^2 \tau_{xy}}{\partial x \partial y} \quad (4.6)$$

By combining the two equations in (4.2) the system is reduced to:

$$\frac{\partial^2 \tau_{xy}}{\partial x \partial y} = -\frac{1}{2}\left(\frac{\partial^2 \sigma_x}{\partial x^2} + \frac{\partial^2 \sigma_y}{\partial y^2}\right) \quad (4.7)$$

which replaced into (4.6) gives the following Laplace equation:

$$\left(\frac{\partial^2}{\partial x^2} + \frac{\partial^2}{\partial y^2}\right)(\sigma_x + \sigma_y) = 0 \quad (4.8)$$

and, therefore, (4.2) and (4.8) along with the corresponding boundary conditions can now be solved for the unknown stresses σ_x , σ_y , and τ_{xy} .

In 1862 Airy had introduced the so-called Airy stress function $\varphi(x, y)$ such that:

$$\begin{cases} \sigma_x = \frac{\partial^2 \varphi}{\partial y^2} - \rho g y \\ \sigma_y = \frac{\partial^2 \varphi}{\partial x^2} - \rho g y \\ \tau_{xy} = -\frac{\partial^2 \varphi}{\partial x \partial y} \end{cases} \quad (4.9)$$

which when replaced into (4.8) gives the Airy equation for φ :

$$\frac{\partial^4 \varphi}{\partial x^4} + \frac{\partial^4 \varphi}{\partial x^2 \partial y^2} + \frac{\partial^4 \varphi}{\partial y^4} = 0 \quad (4.10)$$

The solution to (4.10) for φ will then give σ_x , σ_y , and τ_{xy} from (4.9).

Now we will introduce polar coordinates:

$$\begin{cases} x = r \cos \theta \\ y = r \sin \theta \end{cases}, \begin{cases} r^2 = x^2 + y^2 \\ \theta = \tan^{-1}(y/x) \end{cases}, \begin{cases} \vec{e}_r = \cos \theta \vec{i} + \sin \theta \vec{j} \\ \vec{e}_\theta = -\sin \theta \vec{i} + \cos \theta \vec{j} \end{cases} \quad (4.11)$$

where \vec{i} , \vec{j} , and \vec{e}_r , \vec{e}_θ , are respectively orthonormal tangent systems in Cartesian and polar

coordinates, and $\begin{cases} \frac{\partial r}{\partial x} = \cos \theta, & \frac{\partial r}{\partial y} = \sin \theta \\ \frac{\partial \theta}{\partial x} = -\frac{\sin \theta}{r}, & \frac{\partial \theta}{\partial y} = \frac{\cos \theta}{r} \end{cases}$ which implies that

$$\begin{cases} \frac{\partial}{\partial x} = \frac{\partial r}{\partial x} \frac{\partial}{\partial r} + \frac{\partial \theta}{\partial x} \frac{\partial}{\partial \theta} = \cos \theta \frac{\partial}{\partial r} - \frac{\sin \theta}{r} \frac{\partial}{\partial \theta} \\ \frac{\partial}{\partial y} = \frac{\partial r}{\partial y} \frac{\partial}{\partial r} + \frac{\partial \theta}{\partial y} \frac{\partial}{\partial \theta} = \sin \theta \frac{\partial}{\partial r} + \frac{\cos \theta}{r} \frac{\partial}{\partial \theta} \end{cases}$$

Thus system (4.2), in the absence of any body forces, in polar coordinates becomes:

$$\begin{cases} \frac{\partial \sigma_r}{\partial r} + \frac{1}{r} \frac{\partial \tau_{r\theta}}{\partial \theta} + \frac{\sigma_r - \tau_{r\theta}}{r} = 0 \\ \frac{1}{r} \frac{\partial \sigma_\theta}{\partial \theta} + \frac{\partial \tau_{r\theta}}{\partial r} + \frac{2\tau_{r\theta}}{r} = 0 \end{cases} \quad (4.12)$$

While equations (4.9) and (4.10) become:

$$\begin{cases} \sigma_r = \frac{1}{r} \frac{\partial \varphi}{\partial r} + \frac{1}{r^2} \frac{\partial^2 \varphi}{\partial \theta^2} \\ \sigma_\theta = \frac{\partial^2 \varphi}{\partial r^2} \\ \tau_{r\theta} = -\frac{\partial}{\partial r} \left(\frac{1}{r} \frac{\partial \varphi}{\partial \theta} \right) \end{cases} \quad (4.13)$$

and

$$\left(\frac{\partial^2}{\partial r^2} + \frac{1}{r} \frac{\partial}{\partial r} + \frac{1}{r^2} \frac{\partial^2}{\partial \theta^2}\right) \left(\frac{\partial^2 \varphi}{\partial r^2} + \frac{1}{r} \frac{\partial \varphi}{\partial r} + \frac{1}{r^2} \frac{\partial^2 \varphi}{\partial \theta^2}\right) = 0 \quad (4.14)$$

respectively.

Now consider an axi-symmetric stress distribution in a hollow cylinder under uniform pressure on the inner and outer surfaces (Figure 10). Due to the symmetry of the problem σ_r , σ_θ , $\tau_{r\theta}$, and φ are functions of r only. We consider the following boundary conditions:

$$\begin{cases} \sigma_r(a) = -P_i(t) \\ \sigma_r(b) = -P_e(t) \end{cases} \quad (4.15)$$

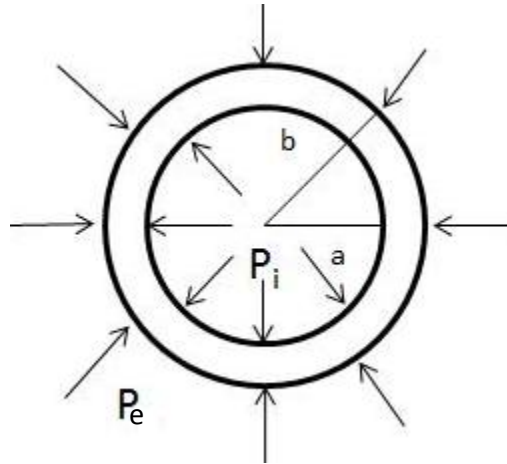


Figure 10: Axi-symmetrical stress distribution in a hollow cylinder under uniform pressure on the inner and outer surfaces.

From [17], the solution that we obtain for the axi-symmetric stress distribution in a hollow cylinder described by the uniform pressure on the inner and outer surfaces (Figure 10) is:

$$\begin{cases} \sigma_r = \frac{a^2 b^2 (P_e - P_i)}{b^2 - a^2} \frac{1}{r^2} + \frac{P_i a^2 - P_e b^2}{b^2 - a^2} \\ \sigma_\theta = -\frac{a^2 b^2 (P_e - P_i)}{b^2 - a^2} \frac{1}{r^2} + \frac{P_i a^2 - P_e b^2}{b^2 - a^2} \end{cases} \quad (4.16)$$

From (4.16) it follows that $\sigma_r + \sigma_\theta = const.$ which means that σ_r and σ_θ produce a uniform extension or contraction in the direction of the axis of the cylinder.

The radial displacement is found now from:

$$\varepsilon_\theta = \frac{u}{r} = \frac{1}{E}(\sigma_\theta - \nu\sigma_r) \quad (4.17)$$

since in the two-dimensional case, the strain tensor in polar coordinates is related to the displacement field $(u, v, 0)$ we get that the strain tensor in polar coordinates is:

$$\left\{ \begin{array}{l} \varepsilon_r = \frac{\partial u}{\partial r} \\ \varepsilon_\theta = \frac{u}{r} + \frac{1}{r} \frac{\partial v}{\partial \theta} \\ \gamma_{r\theta} = \frac{1}{r} \frac{\partial u}{\partial \theta} + \frac{\partial v}{\partial r} - \frac{v}{r} \end{array} \right. \quad (4.18)$$

We replace now equation (4.16) into the inverse form of Hooke's Law in polar coordinates:

$$\left\{ \begin{array}{l} \varepsilon_r = \frac{1}{E}(\sigma_r - \nu\sigma_\theta) \\ \varepsilon_\theta = \frac{1}{E}(\sigma_\theta - \nu\sigma_r) \\ \gamma_{r\theta} = \frac{1}{G}\tau_{r\theta} \end{array} \right. \quad (4.19)$$

where $G = \frac{E}{2(1+\nu)}$ is the modulus of rigidity (or elasticity in shear), use the fact that axisymmetrical cylinder requires $\gamma_{r\theta} = 0$, and get:

$$\frac{\partial u}{\partial r} = \frac{1}{E} \left[\frac{(1+\nu)}{r^2} A + 2(1-\nu)B \ln(r) + (1-3\nu)B + 2(1-\nu)C \right] \quad (4.20)$$

Thus:

$$u(r, \theta) = \frac{1}{E} \left[-\frac{(1+\nu)}{r} A + 2(1-\nu)B r \ln(r) - B(1+\nu)r + 2C(1-\nu)r \right] + f(\theta) \quad (4.21)$$

and

$$\frac{\partial v}{\partial \theta} = \frac{4Br}{E} - f(\theta) \quad (4.22)$$

Integrating (4.22) we get:

$$v(r, \theta) = \frac{4Br\theta}{E} - \int f(\theta)d\theta + g(r) \quad (4.23)$$

Now by replacing both u and v into $\gamma_{r\theta} = 0$ we get that:

$$\frac{1}{r} \frac{df(\theta)}{d\theta} + \frac{dg(r)}{dr} + \frac{1}{r} \int f(\theta)d\theta - \frac{1}{r}g(r) = 0 \quad (4.24)$$

This means that $g(r) = Fr$ and $f(\theta) = H \sin \theta + K \cos \theta$. Therefore,

$$\begin{cases} u(r, \theta) = \frac{1}{E} \left[-\frac{(1+\nu)}{r}A + 2(1-\nu)Br \ln(r) - B(1+\nu)r + 2C(1-\nu)r \right] + H \sin \theta + K \cos \theta \\ v(r, \theta) = \frac{4Br\theta}{E} + Fr + H \cos \theta + K \sin \theta \end{cases} \quad (4.25)$$

with $A, B, C, F, H,$ and K being constants.

However the term $\frac{4Br\theta}{E}$ in the expression of v is multivalued, *i.e.* it changes by 2π as the coordinate θ goes around the circle once; this implies that $B = 0$, since the displacement field must be single-valued.

By imposing the boundary conditions from equation (4.15), it can be shown that:

$$\begin{aligned} \varepsilon_{\theta} &= \frac{1}{E} \left(-\frac{a^2b^2(P_e - P_i)}{b^2 - a^2} \frac{1}{r^2} + \frac{P_i a^2 - P_e b^2}{b^2 - a^2} - \nu \frac{a^2b^2(P_e - P_i)}{b^2 - a^2} \frac{1}{r^2} - \nu \frac{P_i a^2 - P_e b^2}{b^2 - a^2} \right) \\ &= \frac{1}{E} (-1 - \nu) \frac{a^2b^2}{b^2 - a^2} (P_e - P_i) \frac{1}{r^2} + \frac{1}{E} (1 - \nu) \frac{P_i a^2 - P_e b^2}{b^2 - a^2} \end{aligned} \quad (4.26)$$

But from equation (4.18):

$$\varepsilon_{\theta} = \frac{u}{r} + \frac{1}{r} \frac{\partial v}{\partial \theta} \quad (4.27)$$

and since the problem is axi-symmetric with all the involved functions being dependent only on r , it finally follows that:

$$u(r) = \frac{1}{E} (-1 - \nu) \frac{a^2b^2}{b^2 - a^2} (P_e - P_i) \frac{1}{r} + \frac{1}{E} (1 - \nu) \frac{P_i a^2 - P_e b^2}{b^2 - a^2} r \quad (4.28)$$

The above calculations are intended to be used in the numerical simulations describing brain biomechanics, with the application to hydrocephalus. Therefore, it is assumed that the brain

is made of a homogenous, isotropic linear elastic solid which fills a hollow cylinder (Figure 10). It is assumed that P_i is the effective CSF pressure and P_e is the external boundary pressure due to the presence of the skull. Since the intraventricular CSF volume is almost 1.6% of the total brain volume [18], for a cylindrical geometry it follows that $b \sim 8a$. As in [18] where *Hakim et. al.*, [2] investigated a similar problem in the spherical geometry, where they say that the case $b > 8a$ corresponds to abnormally small or slit ventricles, while the case $b < 8a$ corresponds to dilated ventricles – which represents hydrocephalus. When $b \sim a$ the model represents fully developed hydrocephalus.

Now we will be coupling the mechanics of the brain tissue and the CSF dynamics by assuming that $P_i(t)$, the effective CSF pressure in the ventricles, is given either by Marmarou's model or by our Caputo Fractional Marmarou model. In order to make this coupling relevant to clinical applications and address some issues related to Marmarou's model, the following medical facts need to be considered:

- 1) The brain-ventricular CSF interface is made of endothelial cells which are different from the brain's cells (neurons and glia cells) and thus the mechano-chemistry of this interface is different than that of brain tissue.
- 2) The brain-ventricular CSF boundary is stiffer than the brain tissue⁵.

Thus we assume that the brain-ventricular CSF interface is a very thin membrane that separates the ventricles filled with CSF and the brain tissue. For now, we will consider this membrane as part of the brain tissue but with different mechanical parameters. More precisely, the Young's modulus of the brain-ventricular CSF interface is bigger than the Young's modulus of the brain tissue. However, during the evolution of hydrocephalus, as the CSF is accumulating in the ventricles, the brain-ventricular CSF interface will undergo deformation and becomes stiffer until damage occurs.

⁵ Mark Iantosca, pediatric neurosurgeon at Hershey Medical Center, private communication.

4.2 Results

Here we will present plots showing how our fractional model has affected the displacement. We expect that the displacements will follow the trends that were presented above when we displayed the pressure versus time plots. We had found this to be true in [7], so the fractional models should follow the same trend. Since our fractional model for the case of continuous infusion approached the classical solution as α converged 1 the deformations will follow the same trend that was found in [7]; therefore, the plots for this case are not presented here because they do not lead to any further insight. Although, in the case of the bolus injection we have shown that our fractional model does not approach the classical solution, so it is interesting to see if the deformations follow the same behavior.

It can be seen in Figure 11 that in terms of the linear case the displacement of the fractional model agrees with the classical solution, because as α approaches 1 the displacement curves approach the classical curve represented by the solid black line. Although when we

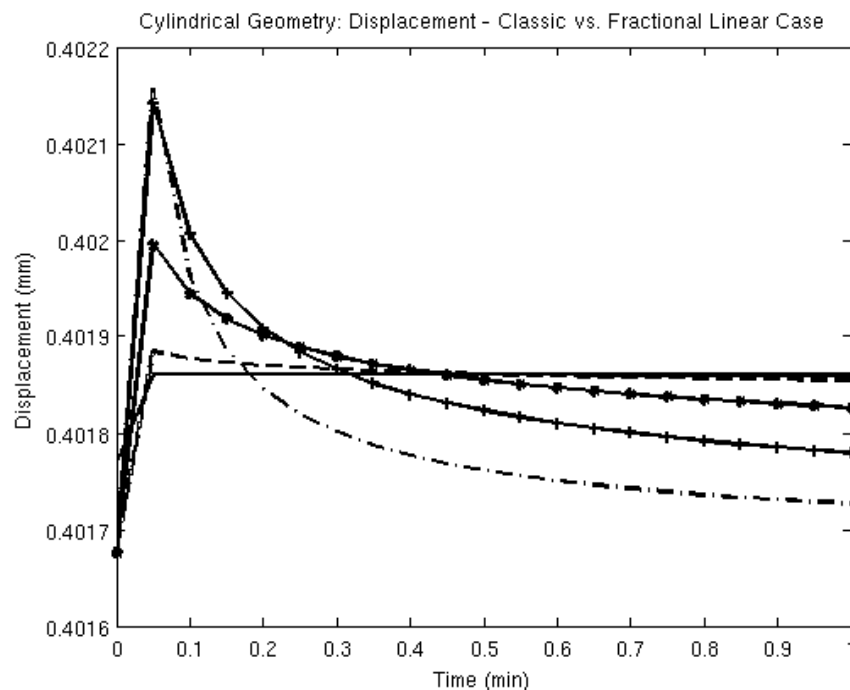


Figure 11: Fractional linear case for bolus injection for α values of: 0.25 (-), 0.5 (+), 0.75 (*), 0.95 (--), 1 (solid). The solid line represents the classical solution.

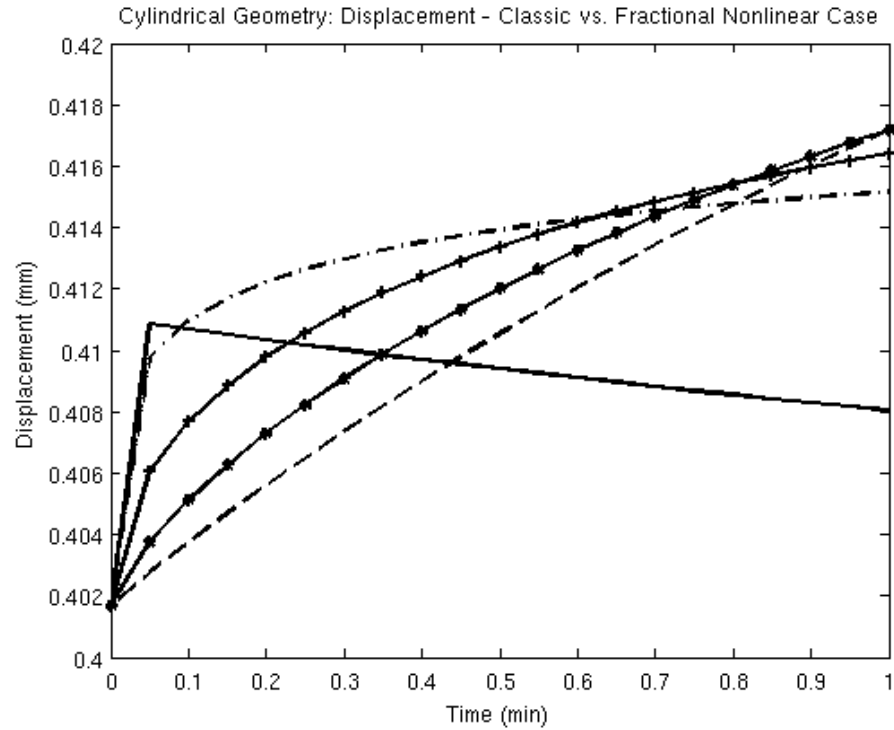


Figure 12: Fractional nonlinear case for bolus injection for α values of: 0.25 (-), 0.5 (+), 0.75 (*), 0.95 (-), 1 (solid). The solid line represents the classical solution.

consider our nonlinear fractional model it does not agree with the classical solution, but does indeed agree with our findings from above. Since our fractional model did not agree in terms of the pressure versus time the displacement curves also do not agree. Given that this was true for the case of continuous infusion it makes sense that it would be the same for the case of bolus injection. In Figure 12 we see the increase in displacement for values of α less than 1, so it appears that a bolus injection of CSF could contribute to the onset of hydrocephalus.

Chapter 5

Brain Biomechanics using Hamilton's Principle

In this chapter we propose a coupled-field model and use Hamilton's principle to investigate the onset and evolution of hydrocephalus.

5.1 Theory

In this section we present a one-dimensional model for brain dynamics using Hamilton's principle. For simplicity, we assume that in the healthy state only small macro-deformations (linear kinematics) can occur in the brain tissue and the mechanical response of the brain tissue at the macroscopic level is linear visco-elastic of Kelvin-Voight type (the stress field in such a material is the sum of a (linear viscous) stress component proportional to the strain rate). The one-dimensional brain tissue of length L has one fixed boundary ($x = 0$) at the interface with the meninges surrounding the brain and one moving boundary ($x = L$) at the interface with the ventricular CSF which undergoes macroscopic displacements caused by the heart pulsations and healthy aging.

We assume further that there are two biological processes happening on different time scales that are important to the proper functionality of the brain: 1) a microstructural healing of the brain and we denote this by $\psi_h(x, t)$ the current healing state function, and 2) a microstructural inflammation of the brain that progresses slowly throughout the entire life and we denote this by $\psi_i(x, t)$ the current inflammation state function. Our second assumption is based on clinical studies [19] that have shown that inflammation plays an important role in the process of normal aging and age-related diseases. In addition, we suggest inflammation of the brain, and,

more specifically, of the choroid plexus (anatomical structure located at the interface between the brain tissue and the ventricular CSF which is involved in the CSF production) as one possible mechanism for the onset of postinfectious and posthemorrhagic pediatric hydrocephalus.

We generalize the theoretical concepts introduced in [20] and adapt them to our model's assumptions. We propose a Lagrangian of the form:

$$\mathcal{L} = \int_0^L \left[\frac{1}{2} m \dot{u}^2 + \frac{1}{2} m \alpha (\dot{\psi}_h^2 + \dot{\psi}_i^2) - \frac{1}{2} \bar{E}(\psi_h, \psi_i) A u'^2 - \frac{1}{2} \beta (\psi_h'^2 + \psi_i'^2) \right] dx \quad (5.1)$$

where m is the mass density of the one dimensional brain tissue of length L and constant cross-sectional area A , $u(x, t)$ is the macroscopic displacement, \bar{E} is the effective macroscopic elastic modulus, and α, β are positive constants for simplicity, but in general α and β will not be the same for each term in the sum so they would not be able to be factored out as we have shown. For simplicity, we denote $\dot{u} = \partial u / \partial t$ and $u' = \partial u / \partial x$. The second and fourth terms of Equation (5.1) represent microstructural kinetics and respectively energies caused by the evolution of the brain's microstructure due to normal healing and inflammation. Similar terms have been proposed before in phase-field models of continua undergoing changes in phase [21,22] and in damage mechanics [20]. As we learn more about the brain, we will improve our definitions and concepts introduced in this model.

As in [20] we defined the virtual work done by non-conservative forces as:

$$\delta \mathcal{W} = \int_0^L [f \delta u - c \dot{u}' \delta u' - \Psi_h(\psi_h, \dot{\psi}_h, \psi_h') \delta \psi_h - \Psi_i(\psi_i, \dot{\psi}_i, \psi_i') \delta \psi_i] dx + F \delta u|_L \quad (5.2)$$

where f is a body force per unit length, $c \dot{u}'$ is the linear damping term of the Kelvin-Voigt model with c the viscosity and Ψ_h, Ψ_i are generalized forces that are work conjugates of the evolution variables ψ_h, ψ_i . Also, F is a concentrated load on the ventricular CSF-brain interface.

We employ now the non-conservative form of Hamilton's principle:

$$\int_{t_1}^{t_2} (\delta\mathcal{L} + \delta\mathcal{W}) dt = 0 \quad (5.3)$$

where the variations in the field variables δu , $\delta\psi_h$, $\delta\psi_i$ are taken to be independent, vanish at the arbitrary times t_1 , t_2 , and satisfy the kinematically admissible geometric boundary conditions.

By definition, the variation of the Lagrangian given by Equation (5.1) is:

$$\begin{aligned} \delta\mathcal{L} &= \frac{\partial\mathcal{L}}{\partial\epsilon} (u + \epsilon\delta u, \psi_h + \delta\psi_h, \psi_i + \delta\psi_i)|_{\epsilon=0} \\ &= \int_0^L \left[m\dot{u}\delta\dot{u} + m\alpha(\psi_h\delta\dot{\psi}_h + \psi_i\delta\dot{\psi}_i) - A\bar{E}u'\delta u' - \frac{1}{2}Au'^2 \left(\frac{\partial\bar{E}}{\partial\psi_h}\delta\psi_h + \frac{\partial\bar{E}}{\partial\psi_i}\delta\psi_i \right) \right. \\ &\quad \left. - \beta(\psi'_h\delta\psi'_h + \psi'_i\delta\psi'_i) \right] dx \end{aligned} \quad (5.4)$$

We replace Equations (5.2) and (5.4) into Hamilton's principle, Equation (5.3), use integration by parts and the facts that the variations δu , $\delta\psi_h$, $\delta\psi_i$ are independent, and vanish at the arbitrary times t_1 , t_2 to obtain the following system of partial differential equations:

$$-m\ddot{u} + A(\bar{E}u')' + f + c\dot{u}'' = 0 \quad (5.5)$$

$$-m\alpha\ddot{\psi}_h - \frac{1}{2}Au'^2 \frac{\partial\bar{E}}{\partial\psi_h} + \beta\psi_h'' - \Psi_h = 0 \quad (5.6)$$

$$-m\alpha\ddot{\psi}_i - \frac{1}{2}Au'^2 \frac{\partial\bar{E}}{\partial\psi_i} + \beta\psi_i'' - \Psi_i = 0 \quad (5.7)$$

We note that Equation (5.7) is in fact the conservation law of linear momentum for our problem of a Kelvin-Voight material of strain u' and stress $A\bar{E}u' + c\dot{u}'$.

To the system created by Equations (5.5) to (5.7) we add boundary conditions:

$$u(0, t) = 0, \quad A\bar{E}u'(L, t) + c\dot{u}'(L, t) = F \quad (5.8)$$

and Dirichlet and/or Neumann boundary conditions at $x = 0, L$ for ψ_h , ψ_i .

We can show now that Equation (5.2) is consistent thermodynamically. If we ignore thermic effects, then the total energy is the sum of all the mechanical energies given in Equation (5.1). We apply the Calusius-Duhem inequality on an arbitrary interval $[x_1, x_2] \subset [0, L]$ and get the following upper bound for the rate of change of the internal energy by the total power of applied forces:

$$\begin{aligned} & \frac{\partial}{\partial t} \int_{x_1}^{x_2} \left[-m\dot{u}^2 + \frac{1}{2}m\alpha(\dot{\psi}_h^2 + \dot{\psi}_i^2) + \frac{1}{2}\bar{E}(\psi_h, \psi_i)Au'^2 + \frac{1}{2}\beta(\psi_h'^2 + \psi_i'^2) \right] dx \\ & \leq \int_{x_1}^{x_2} f\dot{u}dx + F|_{x_1}^{x_2} \end{aligned} \quad (5.9)$$

By taking the time derivative of Equation (5.9), and using Equations (5.5) through (5.7) and integration by parts we transform Equation (5.9) into the following dissipation inequality:

$$\int_{x_1}^{x_2} [c\dot{u}'^2 + \Psi_h\dot{\psi}_h + \Psi_i\dot{\psi}_i]dx \geq [(A\bar{E}u' + c\dot{u} - F)\dot{u} + \beta(\dot{\psi}_h'\dot{\psi}_h + \dot{\psi}_i'\dot{\psi}_i)]|_{x_1}^{x_2} \quad (5.10)$$

From Equation (5.10) we learn that energy is consumed by macroscopic damping as well as by microscopic evolution due to normal healing and inflammation.

Since Equation (5.10) must hold for all sets $\{u', \dot{u}, \dot{u}', \psi_h, \dot{\psi}_h, \dot{\psi}_h', \psi_i, \dot{\psi}_i, \dot{\psi}_i'\}$, we can consider the case when $\dot{u} = \dot{\psi}_h = \dot{\psi}_i = 0$ on the boundaries which reduces Equation (5.10) to:

$$\int_{x_1}^{x_2} [c\dot{u}'^2 + \Psi_h\dot{\psi}_h + \Psi_i\dot{\psi}_i]dx \geq 0 \quad (5.11)$$

Inequality (5.11) must hold for all independent variables $\dot{u}', \dot{\psi}_h, \dot{\psi}_i$ and thus we can finally conclude from Equation (5.11) that:

$$c \geq 0, \quad \Psi_h\dot{\psi}_h \geq 0, \quad \Psi_i\dot{\psi}_i \geq 0 \quad (5.12)$$

Given the complexities of the system formed by Equations (5.5) – (5.7), we start our analysis with the following simple case: $\Psi_h = \Psi_i = F = f = 0$, $\psi_h = \psi_h(t)$, $\psi_i = \psi_i(t)$. In this case Equations (5.5) – (5.7) reduce to:

$$-m\ddot{u} + A(\bar{E}u')' + c\dot{u}'' = 0 \quad (5.13)$$

$$-m\alpha\ddot{\psi}_h - \frac{1}{2}Au'^2 \frac{\partial \bar{E}}{\partial \psi_h} = 0 \quad (5.14)$$

$$-m\alpha\ddot{\psi}_i - \frac{1}{2}Au'^2 \frac{\partial \bar{E}}{\partial \psi_i} = 0 \quad (5.15)$$

Based on experimental and clinical evidence, we can assume further that the brain tissue becomes stiffer during the normal healing period and softer later in life because of aging and thus inflammation becomes predominant. Taking into account these facts and the approach proposed by [20] to study damage mechanics, we introduce the following expression for the effective elastic modulus \bar{E} :

$$\bar{E} = \lambda\psi_h(1 - \psi_i) \quad (5.16)$$

where we assume $\psi_h > 0$, and $0 < \psi_i < 1$. By replacing Equation (5.16) into Equations (5.14) and (5.15) we get:

$$\ddot{\psi}_h = -\frac{\lambda}{2m\alpha}Au'^2(1 - \psi_i) \quad (5.17)$$

$$\ddot{\psi}_i = \frac{\lambda}{2m\alpha}Au'^2\psi_h \quad (5.18)$$

5.2 Application to Hydrocephalus

In order to make some progress in understanding how inflammation could contribute to the onset and development of hydrocephalus using theoretical concepts introduced earlier, we will use the volumetric normal and hydrocephalic mice data published in [23]. For simplicity we take $\frac{\lambda A}{2m\alpha} = 1$ in Equations (5.17) and (5.18).

Since we consider the one-dimensional case, the strain can be calculated as follows:

$$u' = J - 1 \quad (5.19)$$

where the Jacobian of the deformation J is a measure of volume change during the deformation. In Table 2 we provide values for J calculated as the ratio of current brain volume over the initial brain volume, using the brain volumes measured in normal and hydrocephalic given in [23].

Table 2: Calculated Jacobians from brain volumetric data for normal and hydrocephalic mice.

Time (days)	J for normal mice	J for hydrocephalic mice
18	1	1
22	1.032	1.090
23	1.039	1.268
28	1.071	1.280
85	1.250	1.424

We used the built-in Matlab function `polyfit`⁶ to find the following quadratic fitting functions for the data in Table 2:

$$J_n(t) = -0.0001t^2 + 0.0098t + 0.8435 \quad (5.20)$$

for the normal mice data (Figure 13a), and

$$J_h(t) = -0.0004t^2 + 0.0482t + 0.2792 \quad (5.21)$$

for the hydrocephalic mice data (Figure 13b).

⁶ The built in Matlab function `polyfit` uses the least square method to fit a polynomial of given degree through a set of data

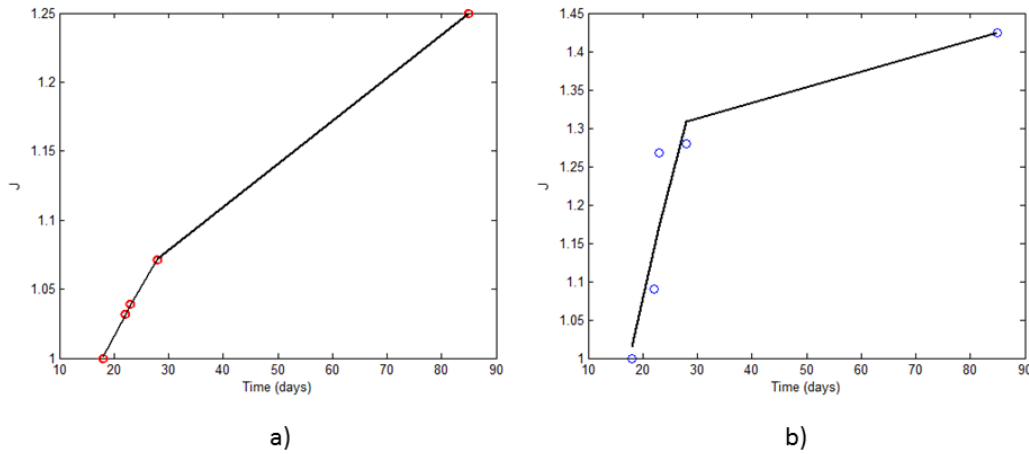


Figure 13: Jacobian for (a) normal (red) and (b) hydrocephalic (blue) mice and their corresponding polynomial fits.

We can now solve Equations (5.17) and (5.18) which, in this case, have the form:

$$\ddot{\psi}_h = -(J_n - 1)^2(1 - \psi_i) \quad (5.22)$$

$$\ddot{\psi}_i = (J_h - 1)^2\psi_h \quad (5.23)$$

In order to integrate the system created by Equations (5.22) and (5.23) using built-in functions in Matlab, we re-write it as a system of first order differential equations as follows:

$$\dot{\psi}_h = v_h \quad (5.24)$$

$$\dot{\psi}_i = v_i \quad (5.25)$$

$$v_h = -(J_n - 1)^2(1 - \psi_i) \quad (5.26)$$

$$v_i = (J_h - 1)^2\psi_h \quad (5.27)$$

We can now use the built-in Matlab function `ode45`⁷ to numerically integrate the system developed from Equations (5.24) through (5.27) for different sets of initial conditions.

⁷ The built-in Matlab function `ode45` uses both fourth and fifth order Runge-Kutta formulas to make error estimates and adjust the time step accordingly.

In Figure 14 we show the temporal variations of healing and inflammation functions for normal and hydrocephalic mice data using the same initial conditions at time $t = 18$ days for both data sets. The sets of initial conditions that we considered here are based on the assumption that in normal mice the rate of healing state function v_h increases fast from birth for a short period of time and then stays constant, while the rate of the inflammation state function v_i increases very slowly throughout the lifespan.

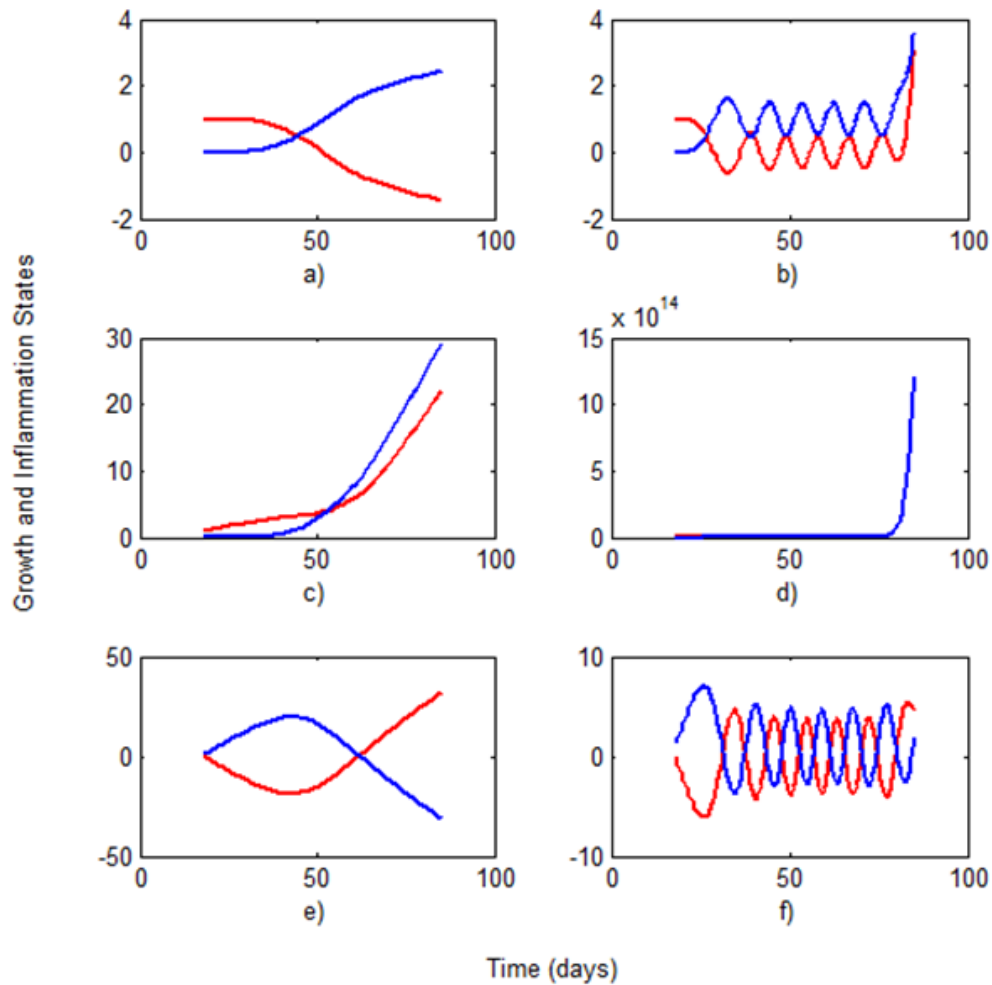


Figure 14: Healing (red) and inflammation (blue) state functions versus time for the following initial conditions: a) – b) $[\psi_h, \psi_i, v_h, v_i] = [1, 0, 0, \text{eps}]$; c) – d) $[\psi_h, \psi_i, v_h, v_i] = [1, 0, 0.1, \text{eps}]$; e) – f) $[\psi_h, \psi_i, v_h, v_i] = [0, 1, -1, 1]$. The first column represents the normal mice data, while the second column shows the hydrocephalic mice data. In Matlab $\text{eps} = 2.2204e - 016$.

For the initial conditions $[\psi_h, \psi_i, v_h, v_i] = [1, 0, 0, eps]$ corresponding initially to no inflammation, constant healing rate, and very small positive inflammation rate; the healing function decreases in time as the inflammation function increases in normal mice (Figure 14a), while in hydrocephalic mice the healing and inflammation state appear to compete with each other (Figure 14b). For the initial conditions $[\psi_h, \psi_i, v_h, v_i] = [1, 0, 0.1, eps]$ corresponding initially to no inflammation, positive healing and inflammation rates; both the healing and inflammation functions increase in time in normal mice with the inflammation function increasing faster in older mice (Figure 14c). However, for these initial conditions, the healing and inflammation functions of hydrocephalic mice blow up (Figure 14d). Lastly, for the initial conditions $[\psi_h, \psi_i, v_h, v_i] = [0, 1, -1, 1]$ corresponding initially to no healing, negative healing rate, positive inflammation rate with both rates having the same magnitude; in normal mice there is an initial decrease in healing followed by an increase, while the inflammation increases initially and after that decreases (Figure 14e). In hydrocephalic mice, we see again the competition between the healing and inflammation states (Figure 14f). From these simulations we could say that the healing function acts more like a natural lifespan healer provided by the immune system. Given that the hydrocephalic mice data are from mice with untreated, induced hydrocephalus, we could hypothesize that in the absence of treatment the natural healing does not have the power to compete alone with the type of inflammation caused by hydrocephalus.

A more detailed analysis into appropriate, clinically relevant initial conditions is however needed in order to fully understand the behaviors seen in Figure 14. Also, a careful mathematical study must be performed on the system developed from Equations (5.24) – (5.27) to understand why it is so sensitive to the given initial conditions when using they hydrocephalic mice data.

Chapter 6

Conclusions and Future Work

In this thesis we have presented a novel pressure-volume model for the CSF dynamics for studying hydrocephalus. We used fractional calculus to generalize Marmarou's model. We believe that our fractional Marmarou model is able to capture some aspects of the brain-CSF interactions which have not been modeled before. Our results show that both a constant infusion and a bolus injection of CSF are possible mechanisms for the onset of hydrocephalus, when we have a fractional order of $\alpha < 0.5$. Further work on our fractional model is needed, in order to improve the convergence of our fractional model. One possibility will be to use Padé approximants as described in [3].

We have also studied the displacements of brain-ventricular CSF interface when the brain tissue is modeled as a linear, isotropic, homogeneous linear elastic solid filling a hollow cylinder bounded by the ventricular CSF in the interior by a rigid skull on the outer boundary. The displacements in this case may be easily calculated. In the case of bolus injection of CSF for $\alpha < 0.5$ the displacements increase suggesting that indeed the CSF bolus injection could contribute to the onset of hydrocephalus.

We have also developed a coupled-field model using Hamilton's principle that has described the healing rate and inflammation rate in both healthy, i.e. normal mice, and hydrocephalic mice. Although there are many computational limitations with our model, it is interesting to notice that in the case of untreated hydrocephalus the healing (or natural growth) of the brain tissue is overpowered by inflammation over time. One way to proceed further is to add to this model pertinent information about treatment. In addition, we could consider a similar system of differential equations as the one developed in [24] describing inflammation in terms of the disease atherosclerosis (a disease that affects the arteries). This system could be adapted to

study hydrocephalus. From [25] we can confirm that the species identified in [24] are also present in diseases that cause inflammation in the brain. This is important because it allows us to either add or delete terms to the system described in [24] based on how prevalent the species are in the brain. The system that was given in [24] is:

$$\dot{I} = Div(\mu_I \nabla I - \chi(I, C) \nabla C) - d_{11}I - a_{15}IL_{ox} - a_{12}ID$$

$$\dot{D} = Div(\mu_D \nabla D) + c_{15}IL_{ox} - a_{21}ID - d_{22}D$$

$$\dot{C} = Div(\mu_C \nabla C) + p_{32}D - a_{31}CI - d_{33}C$$

$$\dot{L} = Div(\mu_L \nabla L) + a_{46}LR - b_4 A_{ox} r_4 L_{ox}$$

$$\dot{L}_{ox} = Div(\mu_{L_{ox}} \nabla L_{ox}) + c_{46}LR - A_{ox} r_4 L_{ox} - b_{15}IL_{ox}$$

$$\dot{R} = Div(\mu_R \nabla R) - b_{46}RL - A_{ox} b_6 R + p_R$$

where I , D , C , L , L_{ox} , and R are immune cells, foam cells, chemo-attractant, native low density lipoproteins, oxidized low density lipoproteins, and free radicals respectively. The terms on the right-hand side of the system above are described in [24]. As stated above the six species that are the basis for these equations are also present when inflammation occurs in the brain. This model is very extensive, but is also very complex and it must be ultimately lined to the mechanics of the brain tissue.

Appendix A

MATLAB Code

Cylindrical deformations:

```
function [ua, ub, ur] = mechanical_disp(P)

a = 4.15; % mm; radius of the ventricular wall calculated from
        % 4*pi/3*a^3=0.3*10^3 mm^3
        % 1mL=10^3 mm^3
b = 8*a; %mm; radius of the entire cylindrical brain
E=1427.58; % Young's modulus units in mmH2O converted from 14kPa
nu=.35; % Poisson's ratio dimensionless
Pe=0; % external boundary condition due to the presence of the skull

% Plot of Cylindrical Geometry modeling Infusion Method
ua=(1/E)*(-1-nu)*( (a.^2*b.^2)/(b.^2-a.^2) ).*(Pe-P)*(1/a)+...
    (1/E)*(1-nu).*( (a.^2.*P-b.^2*Pe)/(b.^2-a.^2) )*a;

ub=(1/E)*(-1-nu)*( (a.^2*b.^2)/(b.^2-a.^2) ).*(Pe-P)*(1/b)+...
    (1/E)*(1-nu).*( (a.^2.*P-b.^2*Pe)/(b.^2-a.^2) )*b;

r = (a+b)/2;
ur =(1/E)*(-1-nu)*( (a.^2*b.^2)/(b.^2-a.^2) ).*(Pe-P)*(1/r)+...
    (1/E)*(1-nu).*( (a.^2.*P-b.^2*Pe)/(b.^2-a.^2) )*r;

end
```

Fractional Model: Constant Infusion:

```
%%%%%%%%%%%%%%%%%%%%%%%%%%%%%%%%%%%%%%%%%%%%%%%%%%%%%%%%%%%%%%%%%%%%%%%%
%
% Classic and Fractional Marmarou Model: Constant Infusion Case
%
%%%%%%%%%%%%%%%%%%%%%%%%%%%%%%%%%%%%%%%%%%%%%%%%%%%%%%%%%%%%%%%%%%%%%%%%
clear all

clc

K=1/0.4343; % units of 1/mL, constant
R=609; % average resistance to CSF absorption calculated from Marmarou
        % paper units of mmH2O/mL/min
```

```

Po=100; % units of mmH2O, normal opening (starting pressure level)
F=.02; % change in I described in Marmarou

t=0:1:100; %t, time measured in minutes

%%%%%%%%%%%%%%%%%%%%%%%%%%%%%%%%%%%%%%%%%%%%%%%%%%%%%%%%%%%%%%%%%%%%%%%%
% constant C; linear ODES
%%%%%%%%%%%%%%%%%%%%%%%%%%%%%%%%%%%%%%%%%%%%%%%%%%%%%%%%%%%%%%%%%%%%%%%%

C = 1/K;

%%%%%%%%%%%%%%%%%%%%%%%%%%%%%%%%%%%%%%%%%%%%%%%%%%%%%%%%%%%%%%%%%%%%%%%%
% Classic case
%%%%%%%%%%%%%%%%%%%%%%%%%%%%%%%%%%%%%%%%%%%%%%%%%%%%%%%%%%%%%%%%%%%%%%%%

P_l_classic = Po+R*F-R*F*exp(-t/(C*R));

figure, plot(t,P_l_classic, 'k');
hold on;

%%%%%%%%%%%%%%%%%%%%%%%%%%%%%%%%%%%%%%%%%%%%%%%%%%%%%%%%%%%%%%%%%%%%%%%%
% Fractional case
%%%%%%%%%%%%%%%%%%%%%%%%%%%%%%%%%%%%%%%%%%%%%%%%%%%%%%%%%%%%%%%%%%%%%%%%

alpha = [0.25, 0.5, 0.75, 0.95];

for i = 1:4

    a0 = Po;
    a1(i) = 1/gamma(alpha(i)+1)*(F/C+Po/(C*R)-a0/(C*R));
    a2(i) = gamma(alpha(i)+1)/gamma(2*alpha(i)+1)*(-a1(i))/(C*R);
    a3(i) = gamma(2*alpha(i)+1)/gamma(3*alpha(i)+1)*(-a2(i))/(C*R);
    a4(i) = gamma(3*alpha(i)+1)/gamma(4*alpha(i)+1)*(-a3(i))/(C*R);

    P_l_frac(:,i) = a0+a1(i)*t.^alpha(i)+a2(i)*t.^(2*alpha(i))+...
        a3(i)*t.^(3*alpha(i))+a4(i)*t.^(4*alpha(i));

end;

plot(t, P_l_frac(:,1), 'r', t, P_l_frac(:,2), 'm',...
    t, P_l_frac(:,3), 'g', t, P_l_frac(:,4), 'b');

hold off;

xlabel('Time (min)');
ylabel('Pressure(Pa)');
title('Infusion Pressures - Linear Classic and Fractional Cases');

clear alpha a0 a1 a2 a3 a4

```

```

%%%%%%%%%%%%%%%%%%%%%%%%%%%%%%%%%%%%%%%%%%%%%%%%%%%%%%%%%%%%%%%%%%%%%%%%
% nonlinear Ricatti ODES
%%%%%%%%%%%%%%%%%%%%%%%%%%%%%%%%%%%%%%%%%%%%%%%%%%%%%%%%%%%%%%%%%%%%%%%%

%%%%%%%%%%%%%%%%%%%%%%%%%%%%%%%%%%%%%%%%%%%%%%%%%%%%%%%%%%%%%%%%%%%%%%%%
% Classic case: Marmarou solution from his paper
%%%%%%%%%%%%%%%%%%%%%%%%%%%%%%%%%%%%%%%%%%%%%%%%%%%%%%%%%%%%%%%%%%%%%%%%

P=(Po*(Po+R*F))./(Po+(R*F).*exp(-(K/R)*(Po+R*F).*t));

figure, plot(t,P, 'k');
hold on;

%%%%%%%%%%%%%%%%%%%%%%%%%%%%%%%%%%%%%%%%%%%%%%%%%%%%%%%%%%%%%%%%%%%%%%%%
% Fractional case
%%%%%%%%%%%%%%%%%%%%%%%%%%%%%%%%%%%%%%%%%%%%%%%%%%%%%%%%%%%%%%%%%%%%%%%%

alpha = [0.1, 0.25, 0.3, 0.35];

beta1 = -K*(F+Po/R);
beta2 = K/R;

for i = 1:4

    a0 = Po;
    A0 = a0^2;

    a1(i) = 1/gamma(alpha(i)+1)*(-beta1*a0-beta2*A0);
    A1(i) = 2*a0*a1(i);

    a2(i) = gamma(alpha(i)+1)/gamma(2*alpha(i)+1)*(-beta1*a1(i)-beta2*A1(i));
    A2(i) = a1(i)^2+2*a0*a2(i);

    a3(i) = gamma(2*alpha(i)+1)/gamma(3*alpha(i)+1)*(-beta1*a2(i)-beta2*A2(i));

    P_frac(:,i) = a0+a1(i)*t.^alpha(i)+a2(i)*t.^(2*alpha(i))+...
        a3(i)*t.^(3*alpha(i));

    rho(i) = 1/abs(a3(i))^(1/(3*alpha(i))); %radius of convergence

end;

plot(t, P_frac(:,1), 'r', t, P_frac(:,2), 'm',...
    t, P_frac(:,3), 'g', t, P_frac(:,4), 'b');
hold off;

xlabel('Time (min)');
ylabel('Pressure (Pa)');
title('Infusion Pressures - Nonlinear Classic and Fractional Cases');

clear alpha a0 a1 a2 a3 A0 A1 A2

```



```

%%%%%%%%%%%%%%%%%%%%%%%%%%%%%%%%%%%%%%%%%%%%%%%%%%%%%%%%%%%%%%%%%%%%%%%%
%
% mechanical displacements: linear case
%
%%%%%%%%%%%%%%%%%%%%%%%%%%%%%%%%%%%%%%%%%%%%%%%%%%%%%%%%%%%%%%%%%%%%%%%%

[ua_lc, ub_lc, ur_lc] = mechanical_disp_2012(P_l_classic);

figure, plot(t, ua_lc, 'r');
hold on, plot(t, ub_lc, 'b');
hold on, plot(t, ur_lc, 'g');
hold off;

xlabel('Time (min)');
ylabel('Displacement (mm)');
title('Cylindrical Geometry: Infusion Displacements - Linear Classic Case');

for i=1:4

    [ua_lf(:,i),ub_lf(:,i), ur_lf(:,i)] = mechanical_disp_2012(P_l_frac(:,i));

end;

figure, plot(t, ua_lc, 'k', t, ua_lf(:,1), 'r', t, ua_lf(:,2), 'm', ...
    t, ua_lf(:,3), 'g', t, ua_lf(:,4), 'b');

xlabel('Time (min)');
ylabel('Displacement (mm)');
title('Cylindrical Geometry: Infusion Displacements - Linear Fractional Case');

%%%%%%%%%%%%%%%%%%%%%%%%%%%%%%%%%%%%%%%%%%%%%%%%%%%%%%%%%%%%%%%%%%%%%%%%
%
% mechanical displacements: non-linear case
%
%%%%%%%%%%%%%%%%%%%%%%%%%%%%%%%%%%%%%%%%%%%%%%%%%%%%%%%%%%%%%%%%%%%%%%%%

[ua_nlc, ub_nlc, ur_nlc] = mechanical_disp_2012(P);

figure, plot(t, ua_nlc, 'r');
hold on, plot(t, ub_nlc, 'b');
hold on, plot(t, ur_nlc, 'g');
hold off;

xlabel('Time (min)');
ylabel('Displacement (mm)');
title('Cylindrical Geometry: Infusion Displacements - Nonlinear Classic Case');

for i=1:4

    [ua_nlf(:,i),ub_nlf(:,i), ur_nlf(:,i)] = mechanical_disp_2012(P_frac(:,i));

```

```

end;

figure, plot(t, ua_nlc, 'k', t, ua_nlf(:,1), 'r', t, ua_nlf(:,2), 'm', ...
            t, ua_nlf(:,3), 'g', t, ua_nlf(:,4), 'b');

xlabel('Time (min)');
ylabel('Displacement (mm)');
title('Cylindrical Geometry: Infusion Displacements - Nonlinear Fractional
Case');

```

Fractional Model: Injection:

```

%%%%%%%%%%%%%%%%%%%%%%%%%%%%%%%%%%%%%%%%%%%%%%%%%%%%%%%%%%%%%%%%%%%%%%%%
%
% Classic and Fractional Marmarou Model: Bolus Injection Case
%
%%%%%%%%%%%%%%%%%%%%%%%%%%%%%%%%%%%%%%%%%%%%%%%%%%%%%%%%%%%%%%%%%%%%%%%%
clear all

clc

K=1/0.4343; % units of 1/mL, constant
R=609; % average resistance to CSF absorption calculated from Marmarou
        % paper units of mmH2O/mL/min
Po=100; % units of mmH2O, normal opening (starting pressure level)
F=.02; % change in I described in Marmarou for cats

%V0 = 120; % units of mL, initial CSF volume in normal humans
V0 = 3; % units of mL, initial CSF volume in normal cats (approx)

V = 0.02; % added volume bolus CHECK THIS VALUE!

t= 0:0.05:1; %t, time measured in minutes

dt = 0.05;

%%%%%%%%%%%%%%%%%%%%%%%%%%%%%%%%%%%%%%%%%%%%%%%%%%%%%%%%%%%%%%%%%%%%%%%%

% Marmarou's solution: does NOT satisfy initial condition and the equation
% at t = 0!!!

P_marmarou = Po*exp(K*V)*exp(K*Po*t/R)./(1+exp(K*V)*(exp(K*Po*t/R)-1)); %
pressure

figure, plot(t,P_marmarou, 'k-', 'LineWidth', 2);
hold on;

```



```

P_l_classic = Po+K*V*exp(-K.*t/R).*heaviside(t);

figure, plot(t, P_l_classic, 'k', 'LineWidth', 2);
hold on;

alpha = [0.25, 0.5, 0.75, 0.95];

for i = 1:length(alpha)

    P_l_frac(:,i) = Po+K*Po/R*(-1/gamma(alpha(i)+1)+...
        1/(alpha(i)*gamma(alpha(i))))*t.^alpha(i)+...
        K^2*Po/R^2*(1/gamma(2*alpha(i)+1)-...
        1/(2*alpha(i)*gamma(2*alpha(i))))*t.^(2*alpha(i))+...
        K*V/gamma(alpha(i)).*t.^(alpha(i)-1)-...
        K/R*K*V/gamma(2*alpha(i)).*t.^(2*alpha(i)-1)+...
        K^2/R^2*K*V/gamma(3*alpha(i)).*t.^(3*alpha(i)-1); % fractional
pressure

end;

P_l_frac(1,:) = Po; % there is an issue in the for loop with t(1)^(alpha-1)
% giving NaN since t(1)=0

plot(t, P_l_frac(:,1), 'r', t, P_l_frac(:,2), 'm',...
    t, P_l_frac(:,3), 'g', t, P_l_frac(:,4), 'b', 'LineWidth', 2);
xlabel('Time (min)');
ylabel('CSF Pressure (mmH2O)');
title('CSF Pressure - Classic and Fractional Linear Case')
hold off;

%%%%%%%%%%%%%%%%%%%%%%%%%%%%%%%%%%%%%%%%%%%%%%%%%%%%%%%%%%%%%%%%%%%%%%%%
%
% mechanical displacements: linear case
%
%%%%%%%%%%%%%%%%%%%%%%%%%%%%%%%%%%%%%%%%%%%%%%%%%%%%%%%%%%%%%%%%%%%%%%%%

[ua_lc, ub_lc, ur_lc] = mechanical_disp(P_l_classic);

for i=1:4

    [ua_lf(:,i),ub_lf(:,i), ur_lf(:,i)] = mechanical_disp(P_l_frac(:,i));

end;

figure, plot(t, ua_lf(:,1), 'k-.', t, ua_lf(:,2), 'k+-',...
    t, ua_lf(:,3), 'k*-', t, ua_lf(:,4), 'k--',...
    t, ua_lc, 'k', 'LineWidth', 2);
xlabel('Time (min)');
ylabel('Displacement (mm)');

```

```

title('Cylindrical Geometry: Displacement - Classic vs. Fractional Linear
Case');

%%%%%%%%%%%%%%%%%%%%%%%%%%%%%%%%%%%%%%%%%%%%%%%%%%%%%%%%%%%%%%%%%%%%%%%%
% non-linear case
%
% use an approximation for Dirac distribution to find the solution to
% our fractional model; cannot use the same approximation as before, namely
% Dirac = lim (eps goes to 0) 1/2*eps*t^(eps-1), due to a singularity at 0
% in an integral we have to evaluate. thus we take for this case the
% following approximation:
% Dirac = lim (eps goes to 0) 1/(2*sqrt(pi*eps))*exp(-x^2/(4*eps))

tt = 1;

Vol_nl_frac_numeric = zeros(length(t),length(alpha));
Vol_nl_frac_numeric(1,:) = V0;

for j = 1:length(alpha)

    h1(j) = 1/(gamma(alpha(j)+1)*gamma(1-alpha(j)))*(-
1/(4*eps*sqrt(eps*pi)))*...
        fgauss_integr(@(s)s.*exp(-s.^2./(4*eps))./(tt-s).^alpha(j),0,tt,4);

    % h1 is a limit as eps goes to 0 and tt goes to 0, too!!

    P_nl_frac_numeric(:,j) = Po + K*V*Po/(gamma(alpha(j)+1)).*t.^alpha(j)+...
        K*V*Po/(gamma(2*alpha(j)+1))*(K*V - K*Po/R +
gamma(alpha(j)+1)*h1(j)).*...
        t.^(2*alpha(j));

    for i =1:length(t)

        dVdt_nl_frac_numeric(i,j) = -1/R*P_nl_frac_numeric(i,j)+...
            V*1/(2*sqrt(pi*eps))*exp(-t(i)^2/(4*eps))+Po/R;

        if (i > 1)

            Vol_nl_frac_numeric(i,j) = Vol_nl_frac_numeric(i-1,j)+...
                dVdt_nl_frac_numeric(i,j)*dt;

        end;
    end;

    rho(j) = 1/abs(K*V*Po/(gamma(2*alpha(j)+1))*(K*V - K*Po/R +...
        gamma(alpha(j)+1)*h1(j)).^(1/(2*alpha(j)))) %radius of convergence
end;

figure, plot(t, P_nl_frac_numeric(:,1), 'k-.',t, P_nl_frac_numeric(:,2), 'k+-
',...
    t, P_nl_frac_numeric(:,3), 'k*-', t, P_nl_frac_numeric(:,4), 'k--',...

```

```

    t, P_numeric, 'k', 'LineWidth', 1.2);
xlabel('Time (min)');
ylabel('CSF Pressure (mmH2O)');
%title('CSF Pressure - Classic and Fractional Non-Linear Case')

figure, plot(t, Vol_nl_frac_numeric(:,1), 'k-.', t, Vol_nl_frac_numeric(:,2),
'k+-',...
    t, Vol_nl_frac_numeric(:,3), 'k*-', t, Vol_nl_frac_numeric(:,4), 'k--',...
    t, Vol_numeric, 'k', 'LineWidth', 1.2);
xlabel('Time (min)');
ylabel('Volume (mL)');
%title('Volume: Classic vs. Fractional Nonlinear Case');

%%%%%%%%%%%%%%%%%%%%%%%%%%%%%%%%%%%%%%%%%%%%%%%%%%%%%%%%%%%%%%%%%%%%%%%%
%
% mechanical displacements: non-linear case
%
%%%%%%%%%%%%%%%%%%%%%%%%%%%%%%%%%%%%%%%%%%%%%%%%%%%%%%%%%%%%%%%%%%%%%%%%

for i = 1:length(t)
    [ua_nlc(i), ub_nlc(i), ur_nlc(i)] = mechanical_disp(P_numeric(i));
end;

[ua_marmarou, ub_marmarou, ur_marmarou] = mechanical_disp(P_marmarou);
figure, plot(t, ua_nlc, 'k', t, ua_marmarou, 'ko', 'LineWidth',2);
hold on, plot(t, ub_nlc, 'b', t, ub_marmarou, 'bo', 'LineWidth',2);
hold on, plot(t, ur_nlc, 'r', t, ur_marmarou, 'ro', 'LineWidth',2);
hold off;

xlabel('Time (min)');
ylabel('Displacement (mm)');
title('Cylindrical Geometry: Displacement - Nonlinear Classic Case');

for i=1:4

    [ua_nlf(:,i),ub_nlf(:,i), ur_nlf(:,i)] =
mechanical_disp(P_nl_frac_numeric(:,i));

end;

figure, plot(t, ua_nlf(:,1), 'k-.', t, ua_nlf(:,2), 'k+-',...
    t, ua_nlf(:,3), 'k*-', t, ua_nlf(:,4), 'k--',...
    t, ua_nlc, 'k', 'LineWidth', 2);
xlabel('Time (min)');
ylabel('Displacement (mm)');
title('Cylindrical Geometry: Displacement - Classic vs. Fractional Nonlinear
Case');

```

Brain Data: Normal:

```

function dbN = brainN( t, bN )

dbN = zeros(4,1);

epsilon = 1;

dbN(1) = bN(3);
dbN(2) = bN(4);
dbN(3) = -(-0.0001*t^2+0.0098*t+0.8435-1)^2*(1-epsilon*bN(2));
dbN(4) = epsilon*(-0.0001*t^2+0.0098*t+0.8435-1)^2*bN(1);

end

```

Brain Data: Hydrocephalic:

```

function dbH = brainH( t, bH )

dbH = zeros(4,1);

epsilon = 1;

dbH(1) = bH(3);
dbH(2) = bH(4);
dbH(3) = -(-0.0004*t^2+0.0482*t+0.2792-1)^2*(1-epsilon*bH(2));
dbH(4) = epsilon*(-0.0004*t^2+0.0482*t+0.2792-1)^2*bH(1);

end

```

Hamilton's Principle Model

```

clear all

%use Mandell et al, 2010 data in table 1 for brain volumes of normal and
%
%hydrocephalic mice

xy_normal = load('brainJ_normal_vol_mice.m');

time_normal = xy_normal(:,1);
vol_normal = xy_normal(:,2);

%plot(time_normal, vol_normal, 'ro', 'LineWidth', 2);

pn = polyfit(time_normal, vol_normal, 2);

%hold on;

```

```

%plot (time_normal, pn(1).*time_normal.^2+pn(2).*time_normal+pn(3), 'k-',
'LineWidth', 2);
%hold off;

%%%%%%%%%%%%%%%%%%%%%%%%%%%%%%%%%%%%%%%%%%%%%%%%%%%%%%%%%%%%%%%%%%%%%%%%

xy_hydro = load('brainJ_hydrocephalus_vol_mice.m');

time_hydro = xy_hydro(:,1);
vol_hydro = xy_hydro(:,2);

%figure, plot(time_hydro, vol_hydro, 'bo');

ph = polyfit(time_hydro, vol_hydro, 2);

%hold on;
%plot (time_hydro, ph(1).*time_hydro.^2 + ph(2).*time_hydro + ph(3), 'k-',
'LineWidth', 2);
%hold off;

%%%%%%%%%%%%%%%%%%%%%%%%%%%%%%%%%%%%%%%%%%%%%%%%%%%%%%%%%%%%%%%%%%%%%%%%
% the system of ODEs is however stiff so dsolve can find the analytic
% solutions but they are very poorly behaved; try numerical solutions

[tN100eps, bN100eps] = ode45(@brainN, [18 85], [1 0 0 eps]);
[tH100eps, bH100eps] = ode45(@brainH, [18 85], [1 0 0 eps]);

[tN101eps, bN101eps] = ode45(@brainN, [18 85], [1 0 0.1 eps]);
[tH101eps, bH101eps] = ode45(@brainH, [18 85], [1 0 0.1 eps]);

[tN01m11, bN01m11] = ode45(@brainN, [18 85], [0 1 -1 1]);
[tH01m11, bH01m11] = ode45(@brainH, [18 85], [0 1 -1 1]);

figure,

subplot(3,2,1)
plot(tN100eps, bN100eps(:,1), 'r', tN100eps, bN100eps(:,2), 'b', 'LineWidth',
2);
xlabel('a');

subplot(3,2,2)
plot(tH100eps, bH100eps(:,1), 'r', tH100eps, bH100eps(:,2), 'b', 'LineWidth',
2);
xlabel('b');

subplot(3,2,3)
plot(tN101eps, bN101eps(:,1), 'r', tN101eps, bN101eps(:,2), 'b', 'LineWidth',
2);
xlabel('c');

```



```
subplot(3,2,4)
plot(tH101eps, bH101eps(:,1), 'r', tH101eps, bH101eps(:,2), 'b', 'LineWidth',
2);
xlabel('d');

subplot(3,2,5)
plot(tN01m11, bN01m11(:,1), 'r', tN01m11, bN01m11(:,2), 'b', 'LineWidth', 2);
xlabel('e');

subplot(3,2,6)
plot(tH01m11, bH01m11(:,1), 'r', tH01m11, bH01m11(:,2), 'b', 'LineWidth', 2);
xlabel('f');

[ax1,h1]=suplabel('Time (days)');
[ax2,h2]=suplabel('Growth and Inflammation States','y');

%
%figure, plot(tN, bN(:,3), 'r', tN, bN(:,4), 'b', 'LineWidth', 2);
%
%figure, plot(tH, bH(:,3), 'r', tH, bH(:,4), 'b', 'LineWidth', 2);
%
```

Bibliography

1. Marmarou, A., Shulman, K., & Rosende, R. M. (1978). A nonlinear analysis of the cerebrospinal fluid system and intracranial pressure dynamics. *Surgical Neurology*, 48, 332-344.
2. Hakim, S., Venegas, J. G., & Burton, J. D. (1976). The Physics of the cranial cavity, hydrocephalus and normal pressure hydrocephalus: Mechanical interpretation and mathematical model. *Surgical Neurology*(5), 187-210.
3. Duan, J.-S., Chaolu, T., & Rach, R. (2012). Solutions of the initial value problem for nonlinear fractional ordinary differential equations by the Rach-Adomian-Meyers modified decomposition method. *Applied Mathematics and Computation*, 218, 8370-8392.
4. Kauffman J., Drapaca C.S. (2013). *A Multiscale Pressure-Volume model of Cerebrospinal Fluid Dynamics: Application to Hydrocephalus*. Proceedings of the ASME 2012 2nd Global Congress on Nanoengineering for Medicine & Biology NEMB 2013.
5. Kauffman J., Drapaca C.S. (2013). *A Fractional Pressure- Volume Model of Cerebrospinal Fluid Dynamics in Hydrocephalus*. Proceedings of the Annual Conference & Exposition on Experimental and Applied Mechanics SEM 2013.
6. Drapaca C.S., Kauffman J.A. (2013). *A Study of Brain Biomechanics using Hamilton's Principle*. Interdisciplinary Conference Series: Applied Mathematics, Modeling, and Computer Science AMMC2013.
7. Kauffman, J. A. (2012). *Simulation of hydrocephalus based on mathematical modeling and technological advancements*. Honors Thesis, The Pennsylvania State University.

8. Czosnyka, M., Czosnyka, Z., Momjian, S., & Pickard, J. D. (2004). Cerebrospinal fluid dynamics. *Physiological Measurement*, 25(5).
9. "Hydrocephalus Association: Brain physiology webpage".
URL <http://www.hydroassoc.org/hydrocephalus-education-and-support/learning-about-hydrocephalus/brain-physiology-relevant-to-hydrocephalus/>
10. Weerakkody, R. A., Czosnyka, M., Schuhmann, M. U., Schmidt, E., Keong, N., & Santarius, T. (2011). Clinical Assessment of cerebrospinal fluid dynamics in hydrocephalus: guide to interpretation based on observational study. *Acta Neurologica Scandinavica*, 124, 85-98.
11. Iliff, J. J., Wang, M., Liao, Y., Plogg, B.A., Peng, W., Gundersen G.A., Benveniste, H., Vates, G.E., Deane, R., & Goldman, S.A. (2012). Facilitates CSF Flow Through the Brain Parenchyma and the Clearance of the Interstitial Solutes, Including Amyloid. *Science Translational Medicine*, 4, p.147ra111.
12. Lundstorm, B. N., Higgs, M. H., Spain, W. J., & Fairhall, A. L. (2008). Fractional differentiation by neocortical pyramidal neurons. *Nature Neuroscience*, 11, 1335-1342.
13. Sherief, H. H., El-Sayed, A., Behiry, S. H., & Raslan, W. E. (2012). *Using Fractional Derivatives to Generalize the Hodgkin-Huxley Model*. (D. Baleanu, J. Machado, & A. Luo, Eds.) New York: Springer.
14. Adomian, G. (1995). Solving the mathematical models of neurosciences and medicine. *Mathematics and Computers in Simulation*, 40, 107-114.
15. Momani, S., & Shawagfeh, N. (2006). Decomposition method for solving fractional Riccati differential equations. *Applied Mathematics and Computation*, 182, 1083-1092.
16. Odibat, Z. M., & Shawagfeh, N. T. (2007). Generalized Taylor's Formula. *Appl. Math. Comp.*(186), 286-293.

17. Timoshenko, S., Goodier, J.N. (1970). *Theory of Elasticity* (3rd ed.). McGraw-Hill Book Company.
18. Brunelle, F. (2004). Modern Imaging of Pediatric Hydrocephalus. In *Pediatric Hydrocephalus* (pp. 79-94).
19. Singh, T., & Newman, A. (2011). Inflammatory markers in population studies of aging. *Ageing Res.Rev*, 10(3), 319-329.
20. Cusumano, J., Roy, A., & Li, Q. (In Preparation). Damage Dynamics, rate laws, and failure statistics via Hamilton's principle. *Royal Society A*.
21. Fried, E., & Gurtin, M. (1993). Continuum theory of themally induced phase transitinos based on an order parameter. *Physica D*(68), 326-343.
22. Fried, E., & Gurtin, M. (1994). Dynamics solid-solid transitions with phase characterized by an order parameter. *Physica D*.(72), 287-308.
23. Mandell, J., Neuberger, T., Drapaca, C., Webb, A., & Schiff, S. (2010). The dynamics of brain and cerebrospinal fluid growth in normal versus hydrocephalic mice. *J. Neurosurg. Pediatrics*(6), 1-10.
24. Ibragimov, A., Ritter, L., & Walton, J. R. (2010). Stability Analysis of a Reaction-Diffusion System Modeling Atherogenesis. *Journal of Applied Mathematics*, 70, 2150-2185.
25. Zheng , W., & Chodobski, A. (2005). *The Blood-Cerebrospinal Fluid Barrier*. Boca Raton, FL: Taylor and Francis Group.